Accepted Manuscript

Shooting three inflammatory targets with a single bullet: Novel multi-targeting anti-inflammatory glitazones

Perihan A. Elzahhar, Rana Alaaeddine, Tamer M. Ibrahim, Rasha Nassra, Azza Ismail, Benjamin S.K. Chua, Rebecca L. Frkic, John B. Bruning, Nadja Wallner, Tilo Knape, Andreas von Knethen, Hala Labib, Ahmed F. El-Yazbi, Ahmed S.F. Belal

PII: S0223-5234(19)30148-5

DOI: https://doi.org/10.1016/j.ejmech.2019.02.034

Reference: EJMECH 11126

To appear in: *European Journal of Medicinal Chemistry*

Received Date: 10 November 2018

Revised Date: 4 February 2019

Accepted Date: 10 February 2019

Please cite this article as: P.A. Elzahhar, R. Alaaeddine, T.M. Ibrahim, R. Nassra, A. Ismail, B.S.K. Chua, R.L. Frkic, J.B. Bruning, N. Wallner, T. Knape, A. von Knethen, H. Labib, A.F. El-Yazbi, A.S.F. Belal, Shooting three inflammatory targets with a single bullet: Novel multi-targeting anti-inflammatory glitazones, *European Journal of Medicinal Chemistry* (2019), doi: https://doi.org/10.1016/j.ejmech.2019.02.034.

Graphical Abstract:

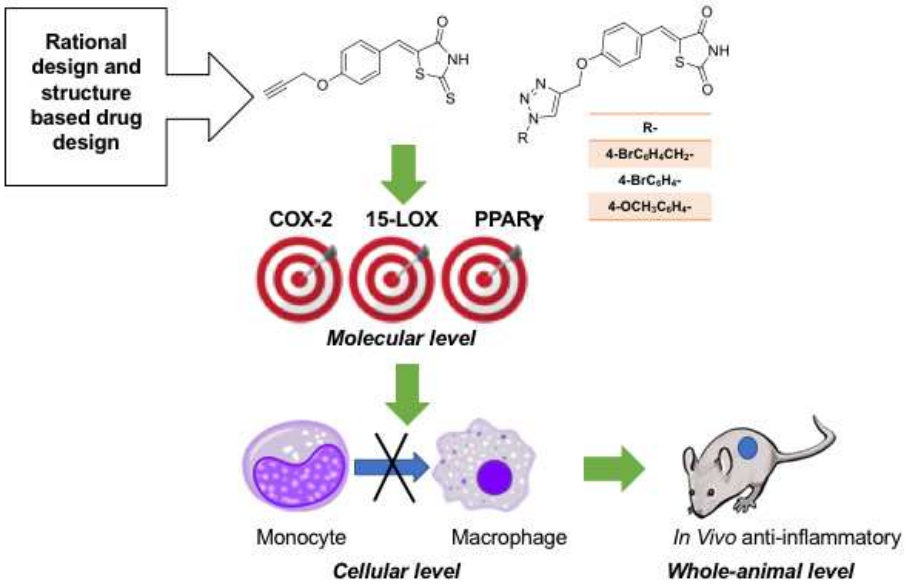

Prototypical balanced modulation of 3 inflammatory targets offered by some novel glitazone-like compounds.

Shooting Three Inflammatory Targets with a Single Bullet: Novel Multi-Targeting Anti-Inflammatory Glitazones

Perihan A. Elzahhar[a], Rana Alaaeddine[b], Tamer M. Ibrahim[c], Rasha Nassra[d], Azza Ismail[a], Benjamin S.K. Chua[e], Rebecca L. Frkic[f], John B. Bruning[f], Nadja Wallner[g], Tilo Knape[g], Andreas von Knethen[g,h], Hala Labib[a,i], Ahmed F . El-Yazbi[b,j*], Ahmed S. F. Belal[a*]

[a]Department of Pharmaceutical Chemistry, Faculty of Pharmacy, Alexandria University, Alexandria 21521, Egypt.

[b]Department of Pharmacology and Toxicology, Faculty of Medicine and Medical Centre, American University of Beirut, Beirut, Lebanon.

[c]Department of Pharmaceutical Chemistry, Faculty of Pharmacy, Kafr-Elsheikh University, Kafr El-Sheikh 33516, Egypt.

[d]Department of Medical Biochemistry, Faculty of Medicine, Alexandria University, Egypt.

[e]School of Biological Sciences, The University of Adelaide, Adelaide, South Australia 5005, Australia.

[f]Institute for Photonics and Advanced Sensing, The School of Biological Sciences, the University of Adelaide, North Tce, Adelaide, South Australia 5005, Australia.

[g]Fraunhofer Institute for Molecular Biology and Applied Ecology IME, Project Group Translational Medicine & Pharmacology TMP, Theodor-Stern-Kai 7, 60596 Frankfurt, Germany.

[h]Institute of Biochemistry I, Faculty of Medicine, Goethe-University Frankfurt, Theodor-Stern-Kai 7, 60596 Frankfurt, Germany.

[i]Department of Pharmaceutical Chemistry, College of Pharmacy, Arab Academy for Science, Technology and Maritime Transport, Alexandria, Egypt.

[j]Department of Pharmacology and Toxicology, Faculty of Pharmacy, Alexandria University, Alexandria 21521, Egypt.

ABSTRACT:

In search for effective multi-targeting drug ligands (MTDLs) to address low-grade inflammatory changes of metabolic disorders, we rationally designed some novel glitazones-like compounds. This was achieved by incorporating prominent pharmacophoric motifs from previously reported COX-2, 15-LOX and PPARγ ligands. Challenging our design with pre-synthetic docking experiments on PPARγ showed encouraging results. *In vitro* tests have identified 4 compounds as simultaneous partial PPARγ agonist, potent COX-2 antagonist (nanomolar IC_{50} values) and moderate 15-LOX inhibitor (micromolar IC_{50} values). We envisioned such outcome as a prototypical balanced modulation of the 3 inflammatory targets. *In vitro* glucose uptake assay defined six compounds as insulin-sensitive and the other two as insulin-independent glucose uptake enhancers. Also, they were able to induce PPARγ nuclear translocation in immunohistochemical analysis. Their anti-inflammatory potential has been translated to effective inhibition of monocyte to macrophage differentiation, suppression of LPS-induced inflammatory cytokine production in macrophages, as well as significant *in vivo* anti-inflammatory activity. Ligand co-crystallized PPARγ X-ray of one of MTDLs has identified new clues that could serve as structural basis for its partial agonism. Docking of the most active compounds into COX-2 and 15-LOX active sites, pinpointed favorable binding patterns, similar to those of the co-crystallized ligands. Finally, *in silico* assessment of pharmacokinetics, physicochemical properties, drug-likeness and ligand efficiency indices was performed. Hence, we anticipate that the prominent biological profile of such series will rationalize relevant anti-inflammatory drug development endeavors.

***Corresponding Authors:**
For AFE: Phone: +961-1-350 000, e-mail: ae88@aub.edu.lb,
ORCID ID: 0000-0003-3432-3038.
For ASFB: Phone: +2-03-4871317, e-mail: ahmed.belal@alexu.edu.eg,
ORCID ID: 0000-0001-9463-0844.

Keywords: Inflammation; Cyclooxygenase-2; 15-Lipoxygenase; Peroxisome proliferator-activated receptor-γ; Multi-targeting.

1. Introduction:

Inflammation is a complex and dynamic response to defend the host against potential threats such as pathogens or tissue insults [1,2]. It is associated with diverse signaling pathways involving enzymes, membrane and cellular receptors, transcription factors and others, operating in an orchestrated manner to counteract the imminent threat [2,3]. Neutrophils and tissue macrophages represent the first line of defense, where they stimulate the production of a plethora of inflammatory mediators as a result of sensing an initial insult [4,5]. Although inflammation is intended to be protective, exaggerated and uncontrollable neutrophil and/or macrophages activity, in addition to failure to achieve resolution often leads to persistent tissue damage, a condition underlying many chronic inflammatory disorders (such as psoriasis, multiple sclerosis, and rheumatoid arthritis) [1].

On the other hand, diabetes is perceived as a multifaceted disease implicating metabolic, cardiovascular, and immune component events; though an understanding of the underlying relating mechanisms are not clear [6,7]. Recent results from our group implicated low-grade adipose inflammation as potential underlying cause of cardiovascular and cardiac autonomic dysfunction associated with metabolic challenge [8]. Indeed, reversal of adipose inflammation was associated with an improved vascular and cardiac autonomic function [8].

Among the different pathways involved in the inflammatory response, arachidonic acid (AA) plays a major role as the biological precursor for many inflammatory mediators. Two key metabolic enzymes are involved in generating AA derivatives, namely: cyclooxygenase (COX) and lipoxygenase (LOX) [9]. COX-2 expression is induced by pro-inflammatory stimuli leading to the generation of inflammatory signaling prostaglandins (PGs) [9,10]. On the other hand, LOXs catalyze the oxygenation of polyunsaturated fatty acids (PUFAs) such as arachidonic and linoleic acids to give oxygenated lipid mediators that are involved in important cellular

signaling mechanisms [11]. Based on the site of oxygenation of arachidonic acid, several mammalian LOX isoforms were discovered and denoted 5-, 12- and 15-LOX [11]. 5-LOX is famous for playing an important role in the pathology of respiratory disorders through the production of 5-hydroperoxy-eicosatetraenoic acid (5-HPETE) which is subsequently converted to leukotrienes (LTs) [11].

Contrarily, 15-LOX converts polyunsaturated fatty acids into 15-*S*-HPETE which is metabolized into either lipoxins or eoxins [11–13]. It is necessary to mention that 5-LOX also contributes to the synthesis of lipoxins [11–13]. While lipoxins are pro-resolving and anti-inflammatory [11–13], eoxins (also referred to as 14,15-LTs) have shown to be pro-inflammatory mediators specially in the context of atherosclerosis, adipocyte differentiation and development of obesity [12,14]. Also, eoxins were shown to have similar actions as leukotrienes, and hence, the probability of their implications in inflammatory and respiratory diseases could not be excluded [12,14]. Moreover, 15-LOX is hypothesized to initiate and/or promote atherosclerosis through LDL oxidation [12,14]. It is not surprising that IL-4 and/or IL-13 induce the expression of 15-LOX in cultured mast cells, monocytes, and epithelial cells [12,14].

Thus, 15-LOX can be regarded as a double-edged weapon that exert both pro- and anti-inflammatory properties and the details of the interplay between them in physiological and pathophysiological contexts are still lacking [12,14]. Up till this moment, various reports indicated that 15-LOX-inhibitors (such as PD146176 among others) could serve as effective therapeutics for a number of 15-LOX-related diseases, which include diabetes, hypertension, obesity, atherosclerosis and other disorders linked to chronic adipose tissue inflammation [14].

The notion of using selective COX-2 inhibitors as anti-inflammatories with minimal gastrointestinal (GI) side effects was very resonating in the late 1990s and early 2000s [15,16]. However, it turned out that blocking only COX-2 would shunt the inflammatory pathways towards more activity of LOX and hence blocking both COX-2 and LOX would provide safer and more effective anti-inflammatory activity [17–19].

Interestingly, *in vitro* studies demonstrated that LOX modulators can activate peroxisome proliferator-activated receptors (PPARs) [20]. Indeed, recent studies *in*

vivo implicated a role for interplay between LOX-derived AA metabolites and PPARγ in mitigating post-ischemic injury in the brain [21]. PPARs are subclasses of the intracellular receptors family, that when activated act as nuclear hormones modulating the transcription of plenty of factors involved in many physiological processes [22–24]. PPARγ activity was first thought to be limited to lipid metabolism and glucose homeostasis [22–24]. However, there is ample evidence demonstrating the role of activated PPARγ in reducing the expression of pro-inflammatory mediators such as cytokines and adhesion molecules involved in neutrophils recruitment to inflammatory foci [23,25]. Moreover, PPARγ agonists were reported to be capable of inhibiting the mRNA expression of COX-2 and nitric oxide synthase (NOS), which further emphasizes the essential role that PPARγ plays in inflammation [23,25,26]. Significantly, clinical trials examining the use of pioglitazone for managing psoriasis, multiple sclerosis, and rheumatoid arthritis are currently ongoing [19].

The last decade has witnessed a paradigm shift in drug discovery programs from designing highly selective single-target ligands to modulating a multiplicity of targets within related signaling networks [27]. Hence, in seeking multi-targeting anti-inflammatory leads with potential future applications in metabolic disorders, we herein report on the development of the first-in-class MTDLs as potential simultaneous COX-2/LOX inhibitors and PPARγ agonists. As a proof of concept, the designed compounds were challenged with different biological assays and *in silico* studies. We believe that the outcomes of this study might aid in expanding the knowledge on the targeting of inflammatory reactions as a valid approach of managing metabolic disorders.

2. Results and discussion:

2.1. Rationale for the design of multi-target directed ligands (MTDLs):

Thiazolidine-2,4-diones (TZDs)/rhodanines constitute diverse scaffolds that are known to exert a vast array of pleiotropic benefits, including insulin-sensitizing, anti-inflammatory and antiproliferative activities [28–30]. They were also reported to prevent the progression of atherosclerotic lesions in patients with type 2 diabetes [31]. Over and above, telmisartan-rosiglitazone hybrid molecules were evaluated as dual

PPARγ agonists/angiotensin II antagonists for management of metabolic syndrome [32]. In particular, TZDs, known as high-affinity PPARγ agonists, have been introduced into clinical practice for the treatment of type 2 diabetes [33].

Thus, in our search for multi-target anti-inflammatory leads with potential efficacy in metabolic disorders, and based on the structural features of four pleiotropic lead compounds; LYSO-7 (**A**) [34,35], pioglitazone (**B**), a reported LOX-inhibiting thiazolidinedione (**C**) [36] and a dual COX-2 / 15-LOX inhibitor (**D**) [37] recently reported by our lab, we adopted a pharmacophoric molecular hybridization approach to design and synthesize some novel triazolyl-thiazolidinedione/rhodanine hybrids as potential simultaneous COX-2/LOX inhibitors and PPARγ agonists. It is worth mentioning that developing a small molecule modulating these 3 targets was not encountered before.

Over and above, the designed assembly has its pharmacophoric parts rooted from pioglitazone. It comprises the essential pharmacophore TZD or its rhodanine bioisostere. This pharmacophore is decorated with a methoxybenzylidene group like compounds **A** and **C** (**Figure 1**), which in turn is connected to the 1,2,3-triazole moiety. This should retain the 3-carbon atom spacer between the oxygen of the phenoxy- linker and nitrogen atom of the pyridine ring (as in pioglitazone) or N-1 of the triazole nucleus (in our designed compounds). Substitution pattern at N-1 of the triazole ring with various aryl and aralkyl groups is attempted to grant variable electronic and lipophilic environments to investigate their effect on the anticipated biological activity and with the hope of achieving better binding interactions with the potential biological targets.

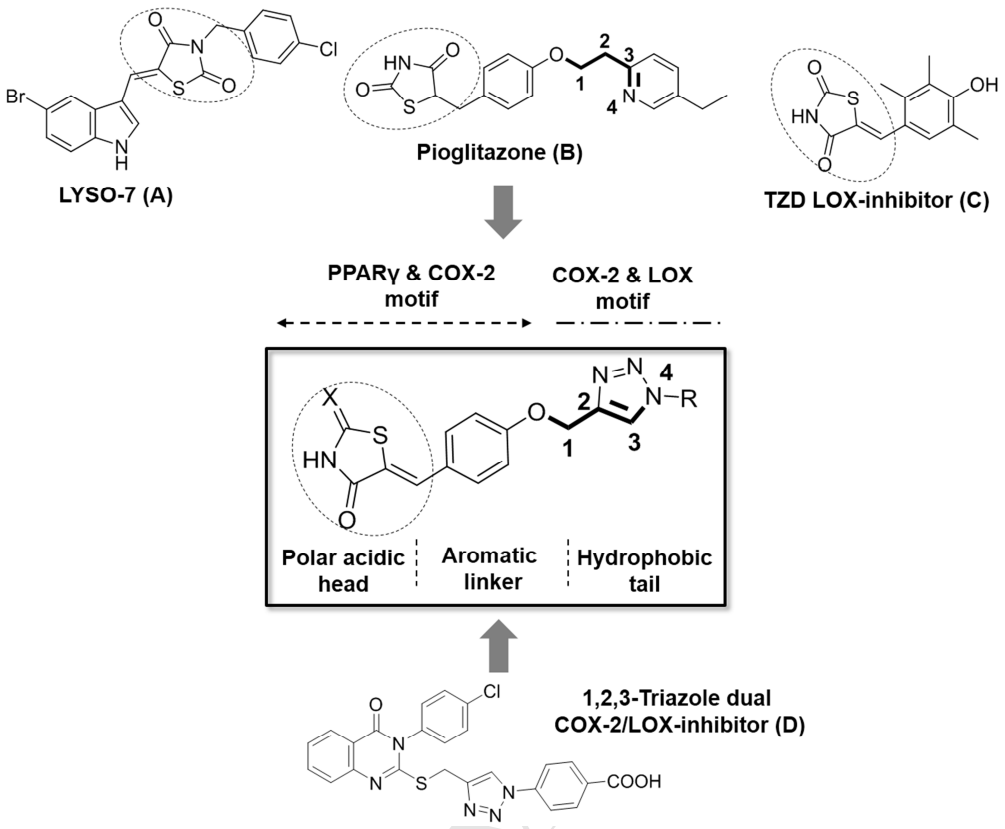

Figure 1. Rationale for the design of the target compounds

In addition, our design agrees with the three-module framework proposed by Pirat *et al.* to represent PPARγ agonist glitazones [38]. It is composed of an acidic polar head group, TZD or rhodanine, joined to a hydrophobic tail through an aromatic linker [38]. We altered the tail group to afford chemical and biological uniqueness while conserving the polar head and the linker regions [38]. Our tail moiety was carefully chosen to be 1,4-disubstituted-1,2,3-triazole which is a pharmacophore we recently reported to show dual COX-2 and LOX inhibitory activity (Structure **D**, **Figure 1**) [37]. Furthermore, target compounds were mapped out with a benzylidene attachment between the polar head and the linker instead of the usual benzyl, which is one distinct difference from pioglitazone (**Figure 1**). We thought that this would be more convenient since recent reports indicated benzylidene TZD derivatives are endowed with partial PPARγ agonistic properties, which retain the desired pharmacological actions while avoiding the untoward adverse effects [39,40].

To the best of our knowledge, the click chemistry-derived 1,4-disubstituted-1,2,3-triazoles have not been explored before for their synchronous PPARγ agonistic and COX-2/LOX inhibitory activities. Together with their wide-ranging biological activities, bioorthogonal nature, being non-classical bioisosteres of the amide group and their propensity to be involved in hydrogen bond and π-π stacking interactions with potential targets [41], it would be tempting to employ this easily accessible structural motif into the aforementioned framework.

2.2.Pre-synthetic PPARγ docking study:

To gain substantial theoretical evidence into the potential PPARγ agonistic activity at the molecular level, molecular docking studies were pre-synthetically applied on 18 compounds that contained our proposed design. Our selection of compounds for PPARγ crystallization and structure determination for *in silico* validation was based on its upstream occurrence in inflammatory pathways (since it is a nuclear receptor), plus its implications in lipid metabolism and glucose homeostasis.

Regarding the chemical structures of the docked compounds, the reader is advised to consult **Scheme 1** using the appropriate coding. Based on literature, the screening performance of PPARγ DEKOIS 2.0 benchmark set employing various docking tools (e.g., GOLD [ChemPLP], Glide [SP] and AutoDock Vina) showed comparable and nonrandom screening performance with all three docking tools [42]. This led us to employ GOLD (ChemPLP) [43,44] as scoring function for pose prediction purposes. Additionally, we employed two additional scoring functions, AutoDock Vina [45] and AutoDock VinaXB [46], for extracting consensus ranking of our proposed compounds.

The crystal structure of PPARγ co-crystallized with rosiglitazone (PDB ID: 2PRG) was used as a model to gauge the binding affinities of the test compounds with the enzyme. The scoring function, hydrogen bonds formed with key amino acids and the relative orientation of the docked compounds with respect to the co-crystallized ligand rosiglitazone were used to estimate the binding propensities to the ligand binding domain (LBD) of PPARγ. Pose-retrieval experiment of the co-crystallized ligand reproduced the key interaction pattern in the binding site of PPARγ with acceptable

RMSD values (e.g., for GOLD docking RMSD = 1.25 Å, **Supplementary Information Figure SM1**).

Examination of the predicted docking scores of the test compounds using GOLD, as indicated in **Supplementary Information Table SM1**, revealed that four compounds were superior to rosiglitazone while other compounds showed slightly lower and comparable scores. According to AutoDock Vina and AutoDock VinaXB, the predicted docking scores (**Table SM1**) almost showed no difference, which excludes halogen-bonding as a possible type of intermolecular interaction between these poses and the backbone of the protein. In addition, all docked compounds showed higher predicted docking scores than the co-crystallized ligand.

The LBD of PPARγ consists of 13 alpha helices and a small beta sheet. Activation function 2 (AF2) is the part of the LBD that is important for ligand dependent coactivator binding and is formed by helices 3-5 and helix 12 [22]. Ser289, His323, His449 and Tyr473 are the most important conserved amino acids that are involved in target recognition of PPARγ ligands [22]. Of particular interest, the formation of a hydrogen bond between a ligand and Tyr473 triggers conformational change in the AF2 site, which enhances the recruitment of coregulatory factors to regulate gene expression [22].

Most of our compounds reproduced the key hydrogen bonding interactions of the co-crystallized ligand (rosiglitazone) via the TZD ring with the residues His449, Gln289, Tyr473, His323 and Ser289, as shown in **Figure 2A** and exemplified by compounds **5e** and **5j**. Moreover, some compounds showed extra binding interactions outside AF2 site as in compound **5j** that formed a hydrogen bond with Ser342.

It is worth mentioning that compounds **5b** and **5g** displayed comparable interaction pattern to rosiglitazone in the binding site of PPARγ via their TZD rings. As well, they showed additional binding interactions with Arg288 and Met264 with the bromophenyl group of **5b** and middle phenoxy group of **5g**, respectively (**Figure 2B**).

Regarding the relative orientation of the compounds in the active site of PPARγ with respect to the co-crystallized ligand, it is clearly evident that the compounds were perfectly accommodated by the LBD and occupied the same position and spatial area

as rosiglitazone (as observed with **5e** and **5j**) (**Figure 2A**). Guided by the above-mentioned data, it was encouraging to synthesize these proposed structures.

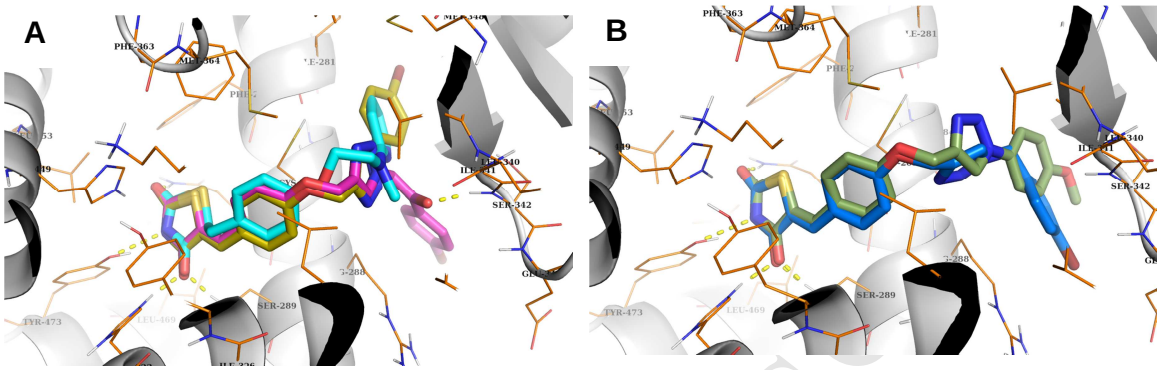

Figure 2. (A) Overlay of the best-scored pose of **5j** (purple) and **5e** (gold) on the co-crystallized ligand (cyan) in the binding site of PPARγ crystal structure (PDB: 2PRG). **(B)** Overlay of the best-scored pose of **5b** (blue) on the pose of **5g** (olive) in the binding site of the PPARγ crystal structure. The yellow dashed-lines represent the polar contacts (H-bonding interactions). Non-polar hydrogen atoms were omitted for clarity.

2.3. Chemistry:

The synthetic strategies for the synthesis of intermediate and target compounds are outlined in **Scheme 1**. The key intermediate 4-propargyloxybenzaldeyhde **(2)** was obtained by the alkylation of 4-hydroxy benzaldehyde with propargyl bromide in the presence of anhydrous potassium carbonate in refluxing dry acetone. Azide-alkyne cycloaddition of compound **2** and the appropriate aromatic azides in the presence of catalytic amount of copper sulfate pentahydrate and sodium ascorbate in DMF/H_2O afforded the desired regioselective 1,4-disubstituted 1,2,3-triazoles (**3a-h**) in good yields comparable to reported ones. Knoevenagel condensation of compounds (**3a-h**) with thiazolidene-2,4-dione or rhodanine in the presence of catalytic amount of piperidine generated the corresponding arylidenes **5a-h** and **6a-h**, respectively. The ^{1}H NMR of **5,6 (a-h)** showed triazole C_5-H aromatic singlet around 8.32-9.15 ppm, along with the characteristic benzylidene CH around 7.58-7.77 ppm. Furthermore, ^{13}C NMR of thiazolidene-2,4-diones (**5a-h**) displayed 2 C=O characteristic peaks at ~168.5 and 160.1 ppm, and benzylidene CH around 143-145 ppm. Additionally, ^{13}C

NMR of rhodanines (**6a-h**) displayed a C=S characteristic peak at ~191.8-196.1 ppm, a C=O characteristic peak at 166.8-173.7 ppm, and benzylidene CH around 143-145 ppm.

Attempts to produce arylidene triazoles **5i-j** and **6i-j** (from phenacyl azides) using the aforementioned method were fruitless. Hence, we decided to adopt an alternative sequence; starting with Knoevenagel condensation to produce arylidenes **4a,b**, which were then subjected to CuAAC to produce the desired compounds **5i-j** and **6i-j**. It is noteworthy to indicate that the latter approach enabled us to screen for the biological activity of arylidenes **4a,b** as well. The ^{1}H NMR of **4 (a,b)** showed a propargylic characteristic triplet in the range of δ 3.61-3.63 ppm, doublet in the range of δ 4.88-4.91 ppm, that corresponds to terminal CH and CH_2, respectively. Both protons underwent a long range coupling of ~2.32 Hz. The ^{13}C NMR of **4 (a,b)** showed propargylic characteristic peaks at δ 56.2, 79.1 and 79.2 ppm corresponding to CH_2, CH and quaternary carbon, respectively. Other characteristic peaks appeared at their expected chemical shifts such as C=O and C=S. The IR spectra of **4 (a,b)** displayed characteristic sharp acetylenic-CH stretching in the range of 3275-3255 cm^{-1} and C≡C stretching in the range of 2376 cm^{-1}. The ^{1}H NMR of **5,6 (i,j)** showed triazole C_5-H aromatic singlet at 8.24 ppm, along with the disappearance of propargylic terminal CH. Furthermore, ^{13}C NMR of **5,6 (i,j)** displayed the triazole C_4 and C_5 peaks, along with the disappearance of previously mentioned propargylic CH and quaternary carbon peaks. Moreover the IR spectra of **5,6 (i,j)** were associated with the disappearance of ethynyl CH and C≡C stretching bands, clearly confirming the formation of the triazole products.

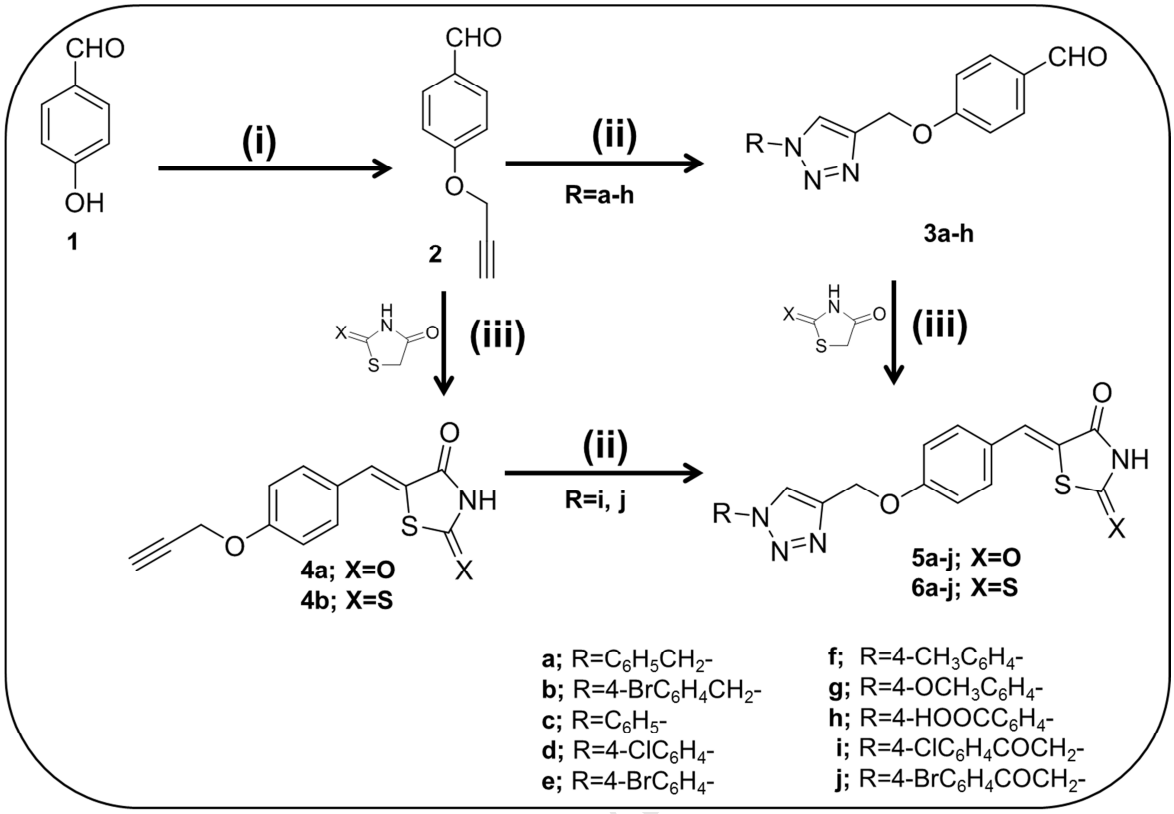

Scheme 1. Synthesis of (*Z*)-5-(4-((1-(aryl or aralkyl)-1*H*-1,2,3-triazol-4-yl)methoxy)benzylidene)thiazolidine-2,4-diones (compounds **5a-j**) or 2-thioxothiazolidin-4-one derivatives (compounds **6a-j**). Reagents and conditions: i) Propargyl bromide, K_2CO_3, Acetone, reflux for 2.5 h. ii) Appropriate azide, $CuSO_4.5H_2O$ (5 mole %), Sodium Ascorbate (20 mole %), DMF/ H_2O, stirring overnight. iii) Piperidine (10 mole%), EtOH, reflux for 12 h.

2.4.Biological evaluation:

2.4.1. *In vitro* COX-1 and COX-2 inhibitory assay:

All synthesized compounds were subjected to an *in vitro* COX-1/COX-2 inhibition assay using an ovine COX-1/human recombinant COX-2 assay kit (Catalog no. 560131; Cayman Chemicals Inc. Ann Arbor, MI, USA).

The half maximal inhibitor concentrations (IC_{50} µM) were determined and the selectivity index (SI) values were calculated as IC_{50} (COX-1)/ IC_{50} (COX-2).

As summarized in **Table 1**; all synthesized compounds, with the exception of compound **5f**, were more potent COX-2 inhibitors than the two reference drugs diclofenac and indomethacin. They also showed higher SI than two reference drugs

diclofenac and indomethacin. Although they showed lower COX-2 inhibition in comparison to celecoxib, they operated within the same range of submicromolar activity.

All compounds inhibited COX-1 in concentrations that are at least one order of magnitude higher than that experienced with COX-2, which highlights the selectivity displayed towards COX-2. Although SI values were lower than that of celecoxib, yet it could be viewed as an advantage by potentially avoiding the cardiovascular side effects of highly selective COX-2 inhibitors [47].

For triazoles prepared from benzyl azides, we observed that the addition of 4-bromo substitution enhanced both COX-2 inhibitory activity and SI values when compared to the unsubstituted analogs. The thiazolidine-2,4-dione derivative **5b** was slightly more potent than the rhodanine **5a**. It reached about 8 times the activity of diclofenac and 5 times that of indomethacin. Intriguingly, **5b** showed the highest SI value (159) out of all the synthesized compounds in the study, which accounts for almost one half that of celecoxib activity and selectivity towards COX-2.

Within the triazole series prepared from aryl azides, it was noticed that 4-substitution with lipophilic π-deficient or π-rich substituents as was seen with 4-bromo (**5e** and **6e**) and 4-methoxy (**5g** and **6g**) remarkably enhanced both COX-2 inhibitory activity and SI values over the unsubstituted congeners. 4-Bromophenyl triazolyl compounds **5e** and **6e** showed about 4-5 times the inhibitory activity of indomethacin with about 950 times its SI towards COX-2. They reached about 6-8 times the inhibitory activity of diclofenac with about 19 times its SI towards COX-2. 4-Methoxyphenyl triazolyl compounds **5g** and **6g** showed about a 3.5-6 times the inhibitory activity of indomethacin with about 700 and 1260 times its SI towards COX-2, respectively. They reached about 5-8 times the inhibitory activity of diclofenac with about 14 and 25 times its SI towards COX-2, respectively.

On the other hand, 4-substitition with methyl (**5f** and **6f**) and carboxylic functionalities significantly reduced COX-2 inhibitory activity and SI values in comparison to their unsubstituted counterparts. Surprisingly, the novel propargyl rhodanine **4b** showed higher COX-2 inhibitory activity and SI value than that of

propargyl thiazolidine-2,4-dione **4a** and was among the most active compounds in the whole study.

Cycloaddition reaction of **4a** and **4b** with 4-substituted phenacyl azides generally enhanced the activity with the highest difference observed with the 4-bromo substituted derivatives **5j** and **6j**.

It is noteworthy that rhodanine derivatives demonstrated superiority in both COX-2 inhibitory activity and SI values in comparison to their thiazolidine-2,4-dione counterparts, with the exception of **5a** and **5b**. A general trend was observed that bromo-containing compounds were among the most active within the whole study.

2.4.2. *In vitro* 15-LOX inhibitory assay:

Compounds that showed the highest *in vitro* COX-2 inhibitory activity (**4b, 5b, 5e, 5g, 5j, 6b, 6e, 6g, 6i** and **6j**) were further subjected to *in vitro* lipoxygenase inhibition assay using soybean 15-LOX assay kit (Catalog no. 760700; Cayman Chemicals Inc. Ann Arbor, MI, USA). Both soybean LOX and human 15-LOX are structurally similar in terms of the presence of both C-terminal catalytic domain and N-terminal membrane binding domain [14]. Also, their catalytic domains display a high level of conservation. More specifically, within 10 Angstrom of the catalytic binding site they show more than 50 % identity [14]. Hence, soybean LOX has been used by a lot of research groups as a valid model to gauge the ability of many novel compounds to inhibit human 15-LOX [14]. *In vitro* 15-LOX enzymatic inhibitory activities are expressed as IC_{50} values of the tested compounds and shown in **Table 1**. The universal LOX inhibitor, nordihydroguaiaretic acid (NDGA)[48,49] and selective 12/15-LOX inhibitor quercetin [50,51] were used as positive controls for comparison. All ten compounds showed substantial LOX inhibitory activity with IC_{50} in the range of 3.14-5.92 µM. They operated in the same order of magnitude as NDGA and quercetin. All ten compounds showed superior LOX inhibitory activity to that of NDGA while displaying varying activity when compared to quercetin. Interestingly, the most and least potent derivatives **4b** and **5b** had almost thrice and twice the activity of NDGA, respectively. Additionally, **4b** was more potent than quercetin while **5e** and **5g** were almost equipotent to quercetin. Other compounds appeared in

the following descending order of activity; **6i**, **5e**, **6b**, **6j**, **5j**, **6g** and **5b**. Consequently, the above results showed that all ten compounds have promising LOX inhibitory activity.

Table 1: *In vitro* COX-1, COX-2, 15-LOX inhibitory IC_{50} values and COX SI values of synthesized compounds.

Code	Structure	IC_{50} µM[a]			SI
		COX-1	COX-2	15-LOX	COX-1/ COX-2[b]
Celecoxib		14.8	0.05	-	296
Diclofenac Na		3.9	0.8	-	4.9
Indomethacin		0.039	0.49	-	0.1
6a	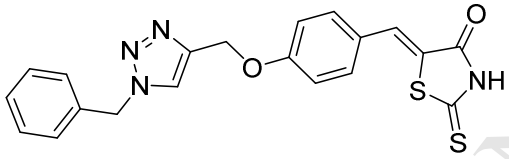	8.4	0.33	-	25.5
5a	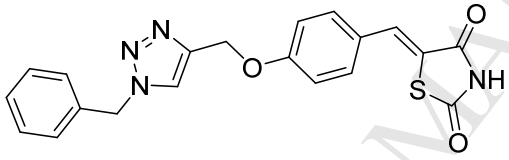	9.4	0.27	-	34.8
6b	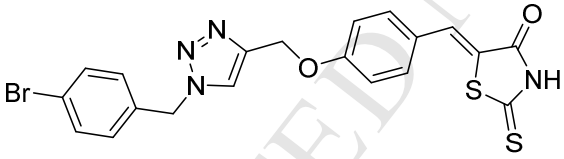	13.4	0.11	4.32	121.8
5b	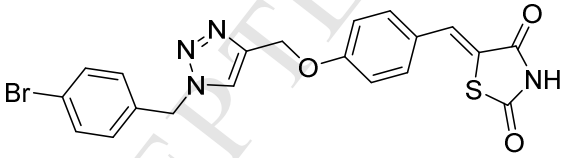	15.9	0.10	5.92	159
6c	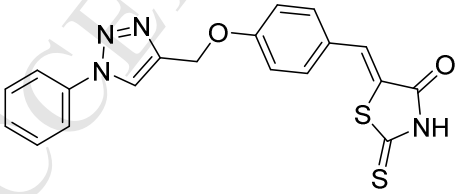	6.4	0.26	-	24.6
5c	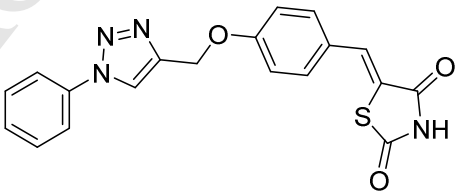	5.9	0.38	-	15.5

6d	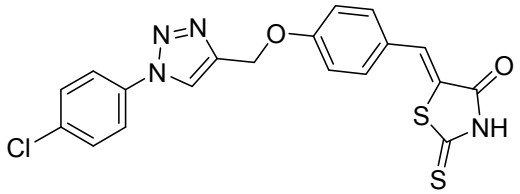	8.6	0.19	-	45.3
5d	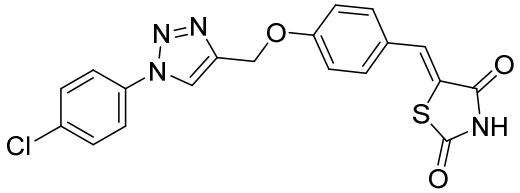	6.9	0.26	-	26.5
6e	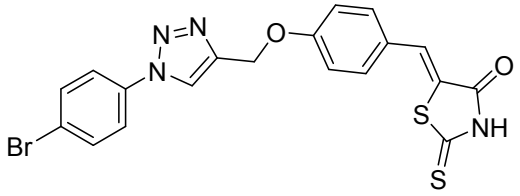	10.5	0.11	3.74	95.5
5e	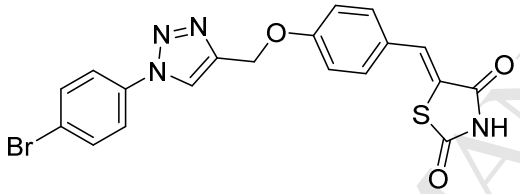	11.6	0.12	4.23	96.7
6f	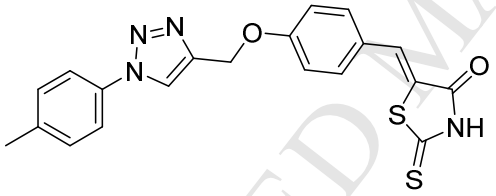	7.4	0.41	-	18.0
5f	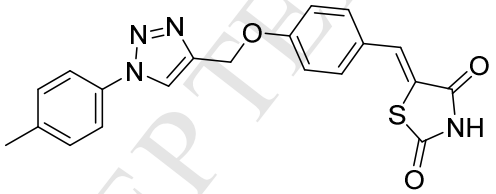	5.9	0.52	-	11.3
6g	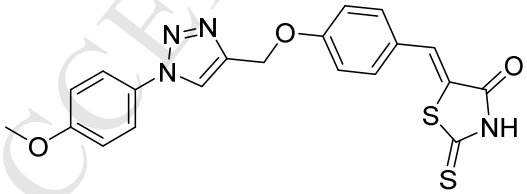	12.6	0.10	5.24	126
5g	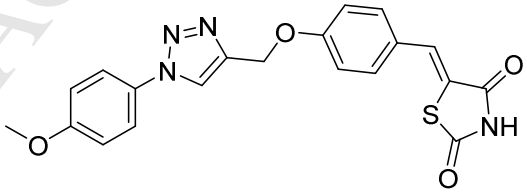	9.8	0.14	3.22	70

6h	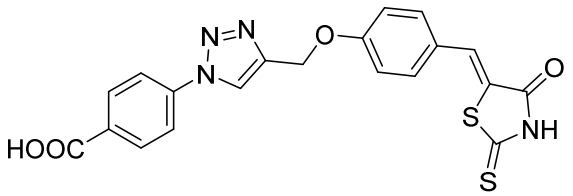	8.2	0.36	-	22.8
5h	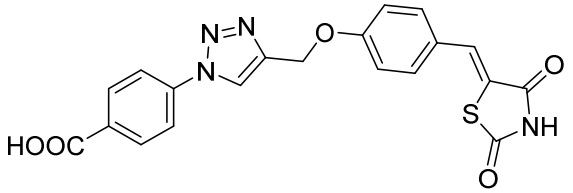	5.9	0.45	-	13.1
6i	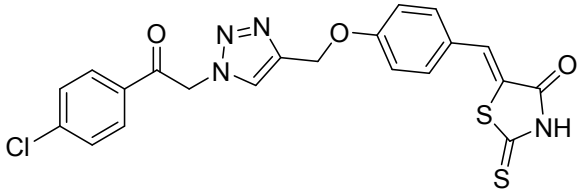	12.4	0.15	4.22	82.7
5i	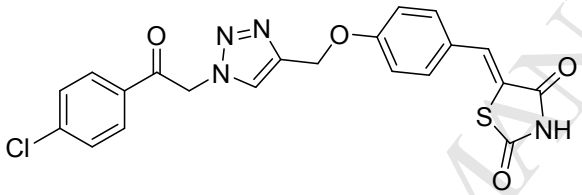	10.9	0.22	-	49.5
6j	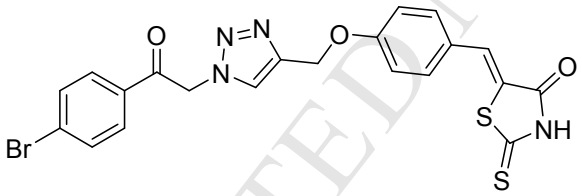	14.9	0.11	4.34	135.5
5j	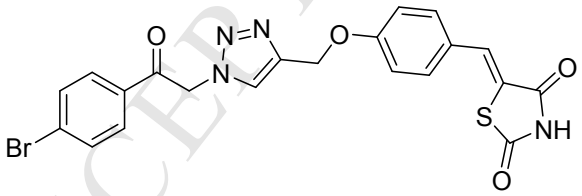	13.6	0.10	4.97	136
4b	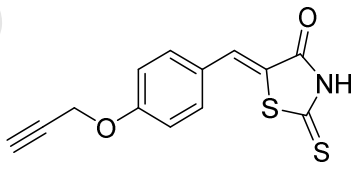	11.6	0.12	3.14	96.7
4a	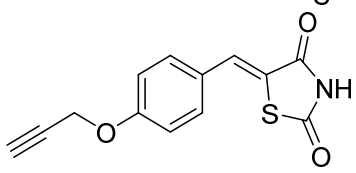	6.9	0.33	-	20.9
NDGA		-	-	10.25	-

Quercetin	-	-	3.27	-

[a]IC_{50} is the concentration (μM) needed to cause 50% inhibition of COX-1, COX-2 and 15-LOX enzymatic activity. All values are expressed as mean of three replicates with standard deviation less than 10% of the mean.
[b]Selectivity index (SI) = IC_{50} (COX-1)/ IC_{50} (COX-2)

2.4.3. *In vitro* glucose uptake using rat hemi-diaphragm model:

In order to assess the antidiabetic activity of compounds that showed the highest *in vitro* COX and LOX inhibitory activities (**4b, 5b, 5e, 5g, 5j, 6b, 6e, 6g, 6i** and **6j**), their glucose uptake potential by rat hemi-diaphragm method was measured as previously reported [31,52,53]. The glucose content of the working solution was measured, and the glucose uptake was calculated as the difference between the initial and final glucose content at 2 mg of optimized drug concentration. The glucose uptake by rat hemi-diaphragm was measured in mg/dl/45 min. Data were expressed as mean ± standard error of mean (SEM) and are shown in **Figure 3**.

Data were analyzed using IBM SPSS software package version 20.0. Statistical analysis was done by ANOVA followed by Tukey *post hoc* test. Results of the *in vitro* glucose uptake assay revealed that compounds **4b, 5e, 6g** and **6j** showed equal or higher glucose uptake than pioglitazone without insulin and significantly higher uptake with insulin. Compounds **5j** and **6i** showed lower glucose uptake without insulin than pioglitazone but equal or higher uptake with insulin. Interestingly, compounds **5b** and **5g** showed equal or higher glucose uptake than pioglitazone in an insulin-independent fashion.

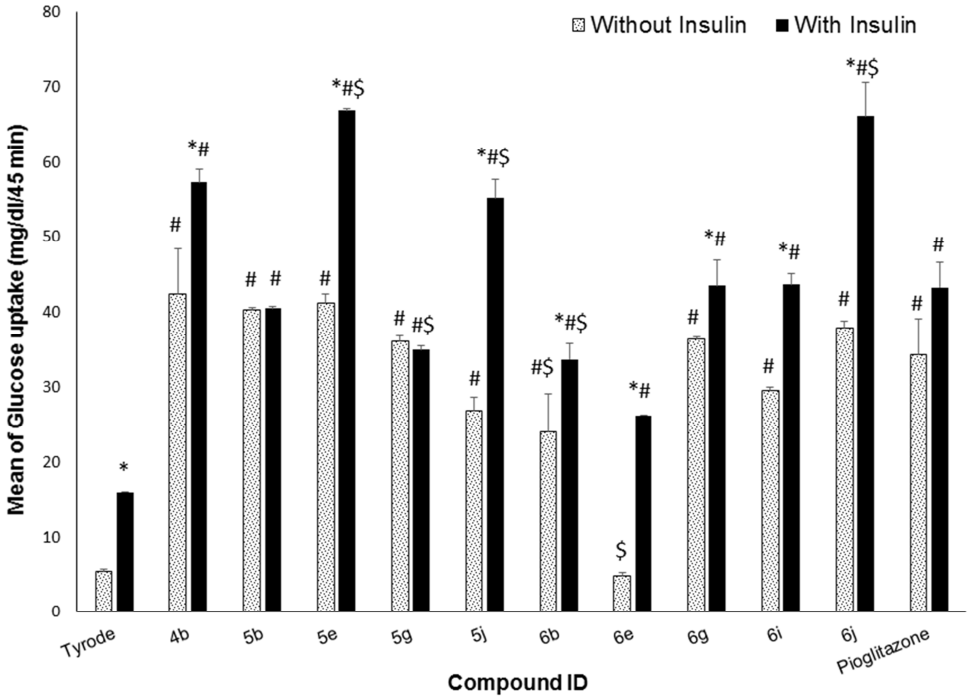

Figure 3. *In vitro* glucose uptake activity of the most active compounds both in absence and presence of insulin using rat hemi-diaphragm model. Data represented are mean ± SD of three replicates. Statistical analysis was performed using Two-way ANOVA followed by Sidak *post hoc* test. A P-value < 0.05 was considered significant. * denotes significance vs. the corresponding effect of each compound in absence of insulin, # denotes significance vs. the corresponding arm of tyrode exposure, while $ denotes significance vs. the corresponding arm of pioglitazone treatment.

2.4.4. Immunohistochemical analysis of ligand-stimulated PPARγ nuclear localization:

PPARγ agonists are known to affect the sub-cellular localization of the receptor increasing its translocation to the nucleus with subsequent regulation of gene expression [54]. The ability of the synthesized compounds to induce PPARγ nuclear translocation was studied in rat primary adipocytes as described previously [21,55]. Four compounds were selected; **4b** & **5e** shown to have an insulin-sensitive glucose uptake effect comparable to pioglitazone, and **5b** & **5g** shown to have a significant insulin-independent glucose uptake. The effect of a 3-hour exposure to 10 μM concentration of each of those compounds on the nuclear localization of PPARγ in rat adipocytes was compared to that of an equivalent concentration of pioglitazone.

Figure 4 shows representative micrographs of control and treated adipocytes. Untreated controls (exposed to an equivalent volume of DMSO as the vehicle) showed diffuse cytosolic PPARγ staining. Adipocytes treated with pioglitazone or the selected test compounds showed redistribution of PPARγ staining that is superimposed with nuclear staining as depicted in the fluorescence intensity profiles along the line scans showed in **Figure 4**. This is suggestive of the ability of the selected compounds to induce PPARγ nuclear translocation similar to pioglitazone. The confirmation of PPARγ nuclear translocation together with insulin-independent glucose uptake of compounds **5b** & **5g** raise the possibility of selective targeting of signaling pathways. We viewed such behavior as an analogy to the phenomenon of biased signaling that has been extensively described for GPCRs [56,57]. Theoretically speaking, the concept of signaling selective agonism can be applied to any multi-signaling receptor, yet and up to our knowledge, compounds **5b** and **5g** are the first small molecule compounds reported to exhibit such behavior on PPARγ.

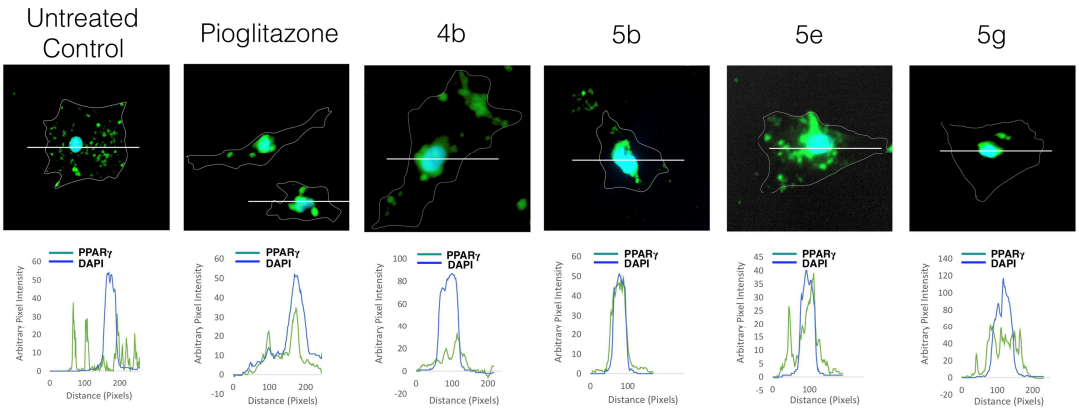

Figure 4. Immunofluorescent staining of PPARγ in untreated rat primary adipocytes and those exposed to 10 µM of pioglitazone and different test compounds for 3 hours. Phase contrast cell contours are delineated in white. Nuclei were stained with DAPI. The corresponding graphs show staining intensity for PPARγ (green) and DAPI (blue) along the scan line indicated on the corresponding micrographs.

2.4.5. PPARγ functional reporter gene assay:

The effect of the selected compounds showing PPARγ nuclear translocation on its transcriptional activity was assessed using a functional gene reporter assay[58]. Human embryonic kidney (HEK293) cells transiently transfected with two components: 1) a hybrid receptor comprising the N-terminal Gal4 DNA binding

domain fused to the ligand binding domain of human PPARγ and 2) reporter Renilla luciferase gene functionally linked to the Gal4 upstream activation sequence. The transfected HEK293 cells were exposed to different concentrations of pioglitazone, **4b**, **5b**, **5e**, and **5g** for 24 hours. Luciferase activity was measured and compared to basal activity in cells treated with the vehicle (DMSO). As shown in **Figure 5**, at the highest concentration (10 μM), pioglitazone showed a 6-fold increase in luciferase activity compared to vehicle. At the same concentration, the tested compounds showed a 2-3 fold increase, with transcriptional activity of 25-45% that of pioglitazone. Based on the transcriptional response, a partial PPARγ agonistic activity can be assumed for the tested compounds.

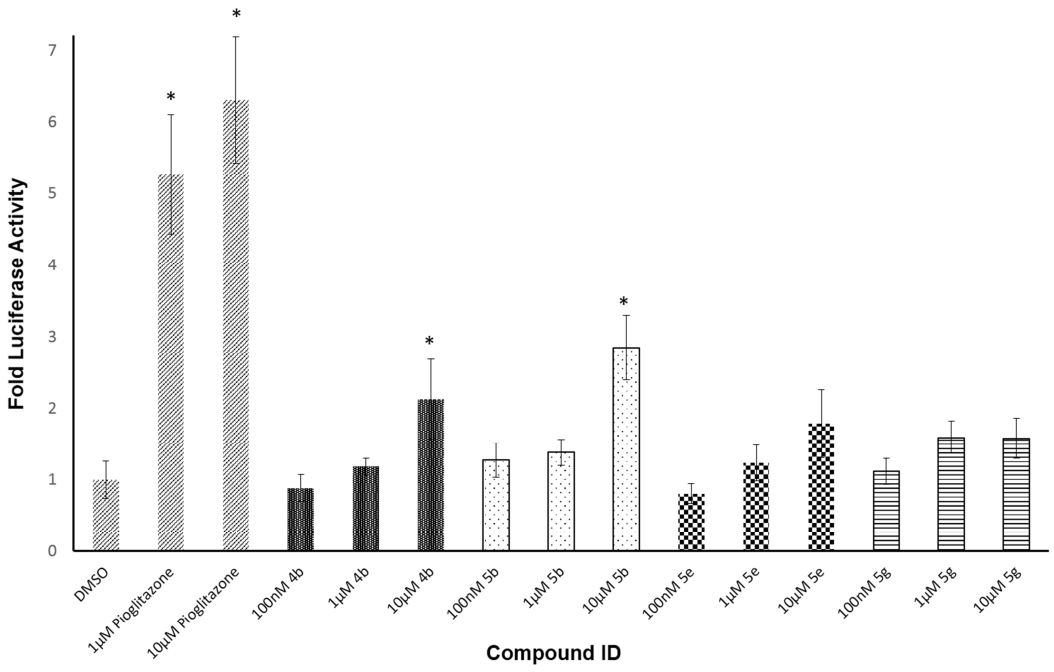

Figure 5. Graphical representation of the increased PPARγ-mediated transcriptional activity following treatment with different concentrations of pioglitazone and selected synthetic compounds. Results are expressed as fold change compared to luciferase activity in vehicle-treated cells and represented as Mean ± Standard deviation. Luciferase activity values were compared to vehicle with One-way ANOVA followed by Dunett Multiple Comparisons test. * denotes a P-value < 0.05 vs. DMSO treated cells.

2.4.6. Inhibition of monocyte to macrophage differentiation:

It is widely recognized that early stages of the inflammatory response involve monocyte-to-macrophage differentiation [59]. This process was shown to be particularly important in the development of atherosclerosis [60]. Interestingly, pioglitazone was shown to modulate the M1/M2 monocyte differentiation imbalance in obese diabetic patients increasing the putative anti-inflammatory M2 polarization, and this effect was postulated to underlie its glucose-independent anti-atherogenic activity [61,62]. Additionally, COX-2 expression is induced during monocytes activation into macrophages with subsequent contribution to the inflammatory response and oxidant/anti-oxidant cellular imbalance [63,64]. Of particular interest, prostaglandin E2, via its action on EP2 and EP4 receptors, was shown to stimulate the production and release of Interleukin-10 (IL-10), a cytokine with reprogramming effects on monocytes and macrophages [65]. Moreover, macrophage activation and adhesion was shown to be dependent on 15-LOX activation [66]. Our previous studies showed that compounds with dual COX-2 and LOX inhibitory activity were able to inhibit monocyte-to-macrophage differentiation[37]. As such, we anticipated that the four compounds (**4b, 5b, 5e, and 5g**) that showed dual COX-2 and LOX inhibitory activities together with PPARγ partial agonistic activities, would maintain a similar, if not enhanced, activity against THP-1 monocyte differentiation into macrophages. Towards this end, we used the PMA-induced THP-1 differentiation assay as an accepted *in vitro* model of this process [67]. The effects of these compounds in the assay were compared to diclofenac and pioglitazone as reference compounds. Results and IC_{50} values are summarized in **Figure 6**. Surprisingly, pioglitazone did not produce an appreciable inhibition of PMA-induced monocyte differentiation up to 300 μM concentration. **5g** produced effects similar to pioglitazone yielding IC_{50} values in the mM range. Diclofenac produced a concentration-dependent inhibition of the differentiation process yielding an IC_{50} value close to that previously reported in a similar assay[37]. **5b** and **5e** showed IC_{50} values close to that of diclofenac, while **4b** appeared to be more potent than diclofenac in inhibiting this process. Yet, it is worth mentioning that this assay measures the differentiation of monocytes into adherent macrophages with no indication of potential differences in differential polarization, if

any. Thus, a negative result might not completely rule out the beneficial effect of PPARγ agonistic activity represented by pioglitazone.

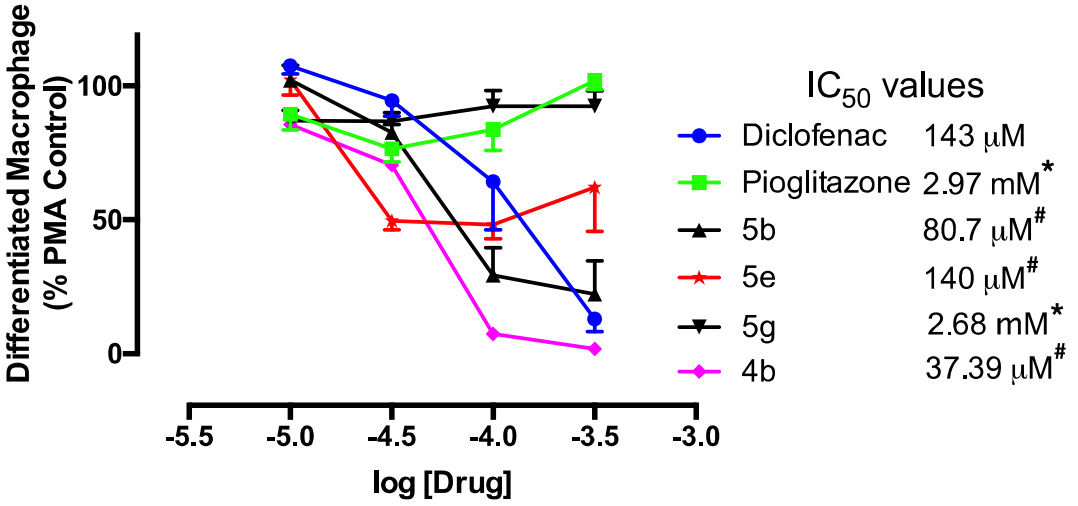

Figure 6. Inhibition of monocyte to macrophage differentiation by diclofenac, pioglitazone, and the selected synthetic compounds. Results are represented as percentage macrophage metabolic activity of the PMA control at different exposure concentrations. IC_{50} values estimated by non-linear regression were compared using One-way ANOVA followed by Tukey Multiple Comparisons *post hoc* test. * denotes a P-value < 0.05 vs. diclofenac while # denotes a P-value < 0.05 vs. pioglitazone.

2.4.7. IL-1β and TNF-α expression and 20-HETE production assay:

Previous literature consistently showed that 15-LOX activation is associated with increased cytokine production in variety of cell types [68–70]. Specifically, both the addition of 15-LOX arachidonate metabolites or their *de novo* synthesis in monocytes triggered cytokine production in macrophages, including tumor necrosis factor-α (TNF-α), interleukin-1β (IL-1β), IL-6, and monocyte chemo-attractant protein-1 [71]. Moreover, the produced IL-1β contributes to further stimulation of signaling pathways leading to the enhancement of phospholipase A2-mediated arachidonate release and metabolism in a positive feedback loop [72]. We attempted to provide a pathophysiological context for the 15-LOX inhibitory action of our hybrid compounds. We examined the effect of the three compounds showing the highest activity against soybean LOX *in vitro* (**4b**, **5e** & **5g**) on TNF-α and IL-1β production in THP-1 monocytes differentiated into macrophages by PMA, and activated by a

lipopolysaccharide (LPS) challenge. Compared to the negative control, LPS-treated macrophages showed massive increases in both TNF-α and IL-1β production **Figure 7A**. The increase in both cytokines' expression was greatly attenuated in cells treated with our compounds. As well, we tested the effect of these compounds on the 20-hydroxyeicosatetraenoic acid (20-HETE) production in these cells as a general indicator of arachidonate metabolism. The concentration of 20-HETE produced in the conditioned medium of PMA-differentiated THP-1 monocytes that were challenged with LPS was measured by enzyme-linked immunosorbent assay (ELISA). 20-HETE production increased following LPS challenge compared to untreated controls. Cells treated with our compounds showed reduced 20-HETE production indicating a possible decrease in arachidonic acid release possibly as a result of the interruption of the IL-1β positive feedback loop (**Figure 7B)**.

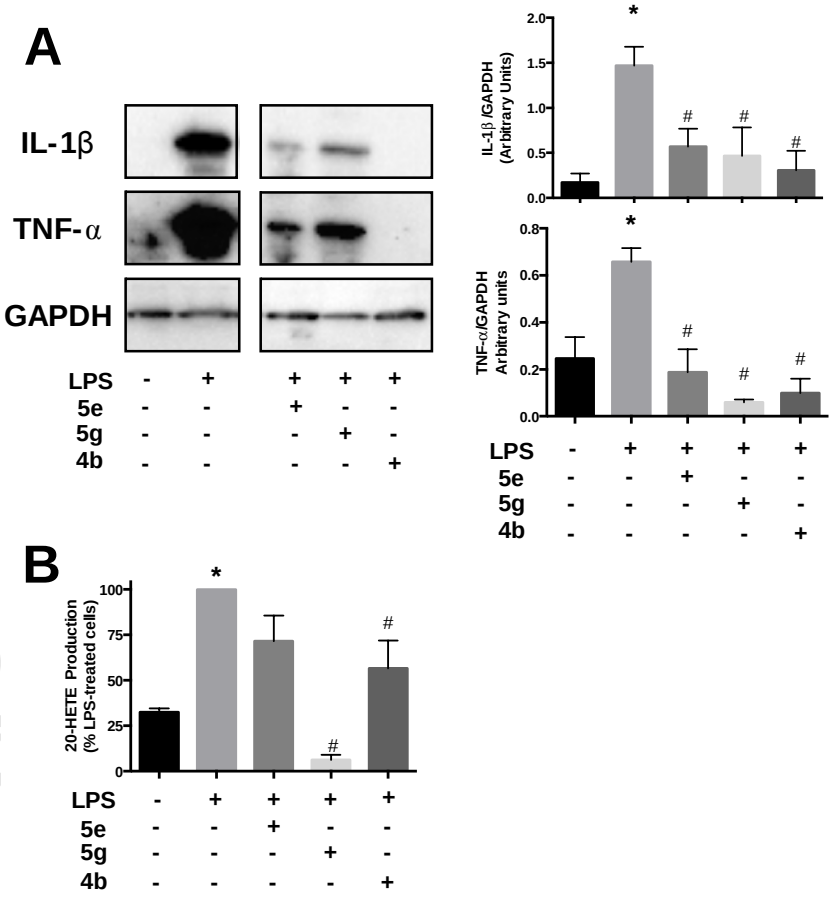

Figure 7. The most potent 15-LOX inhibiting compounds reduce cytokine production and arachidonate metabolism in LPS-challenged PMA-differentiated THP-1 cells. A, representative western blotting of IL-1β, TNF-α, and GAPDH from THP-1 cells

exposed to different treatment conditions. The bar graphs summarize the quantification of three separate experiments. B, 20-HETE concentration in the conditioned medium of THP-1 cells exposed to the indicated treatment conditions. Concentration is normalized to the values measured in untreated cells challenged with LPS. Statistical significance was measured by one-way ANOVA followed by Tukey Multiple Comparisons *post hoc* test. * denotes a P-value < 0.05 vs. untreated control while # denotes a P-value < 0.05 vs. LPS-challenged cells.

2.4.8. *In vivo* anti-inflammatory assay:

Formalin-induced rat paw edema protocol as an acute inflammation model was used to test the *in vivo* anti-inflammatory activity of the four most active compounds **(4b, 5b, 5e and 5g)**. Formalin was injected subcutaneously to induce inflammation and an oral dose of 5 mg/kg body weight of the test compounds was administered.

The potencies of the tested compounds relative to the negative control were identified by measuring the percentage inhibition of edema after 4 h. Celecoxib and diclofenac sodium were used as positive controls. Intriguingly, all tested compounds with the exception of **4b** showed equivalent inhibitory effect to celecoxib and diclofenac. Additionally**, 4b** demonstrated a statistically significant higher potency compared to celecoxib (**Supplementary Information Table SM2** and **Figure 8**).

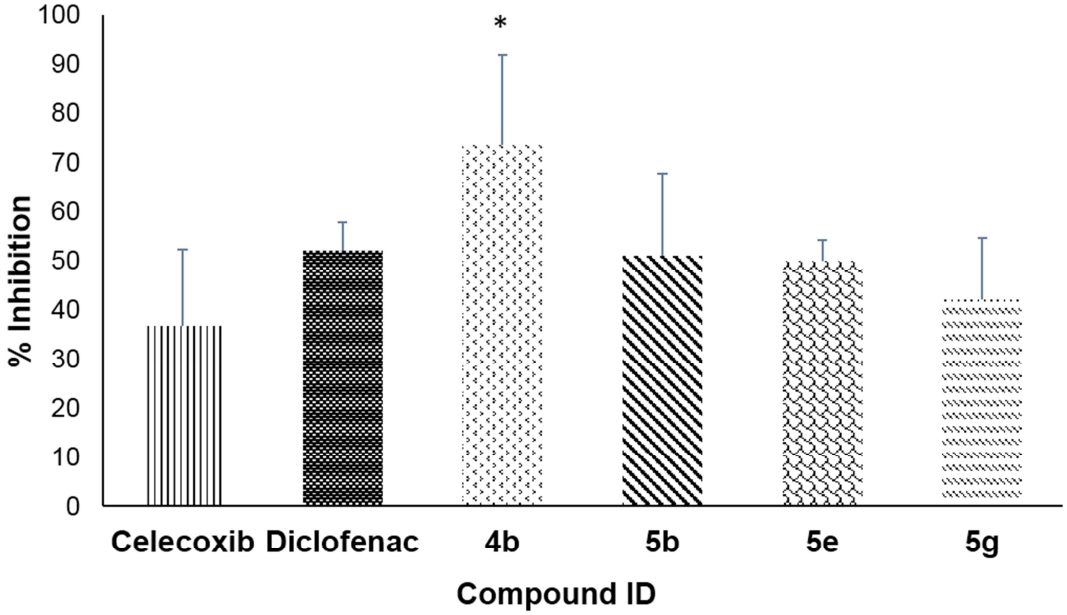

Figure 8. Graphical representation of *in vivo* anti-inflammatory activities of selected compounds in formalin-induced rat paw edema bioassay (acute inflammation model).

Results presented are Mean ± SD of four replicates. Statistical analysis was performed using One-way ANOVA followed by Tukey post hoc test. A P-value < 0.05 was considered significant. * denotes significance vs. celecoxib.

2.5. Structure determination of compound 4b bound to PPARγ:

Recently, 5-ene rhodanine substructures have been stigmatized by some research groups and drug discovery programs as promiscuous hitters or pan assay interference (PAINS) elements [30]. However, the concept of PAINS is still controversial and, in many instances, contradicts the concept of privileged scaffolds [73,74]. Additionally, recent reports indicated that PAINS is highly structural context dependent [73]. Indeed, one of the most active compounds in this study (compound **4b**) carries the ene rhodanine substructure. Although the biological activity of **4b** was confirmed by multiple lines of evidences (molecular then cellular and finally *in vivo*), we wanted to rule out any skepticism about its proven biological activity and exclude the presence of any assay artifacts. Hence, we determined the X-ray crystal structure of compound **4b** in complex with the PPARγ ligand binding domain (LBD) which will give us the chance to probe its binding mode and detect specific binding interactions. Coordinates and structure factors were deposited in the Protein Data Bank under accession code 6E5A.

Experimental details can be found in the methods section, the crystallographic data table describing the data processing and refinement statistics can be found in the **Supplementary Information Table SM3**, and a stereo figure displaying the quality electron density around the ligands can be found in the **Supplementary Information Figure SM2**. Two subunits per asymmetric unit were found and both subunits were found bound to 4b in a similar manner. The overall fold of PPARγ was similar to most other observed structures, for example the **4b** bound structure displays an RMSD to the rivoglitazone bound structure (PDB:5U5L) of 0.48Å (over 512 Cα atoms), signifying that the binding of compound **4b** does not induce major conformational changes as compared to other TZD based compounds. Compound **4b** is located in the LBD with the ring systems of the compound located between H3 and the beta-sheet region and the carbon tail inserted into the hydrophobic patch below the AF2 region (**Figure 9A**). **4b** makes only one hydrogen bond to PPARγ, via its non-protonated

nitrogen atom to the protonated nitrogen backbone atom of Ser342 (3.0Å). All other contacts are hydrophobic and Van der Waals interactions. The double ring system of compound **4b** sits between H3 and the beta sheet region making these contacts with Ile281 (H3), Ile341 side chain (beta-sheet), the non-polar portion of Ser342 side chain (beta-sheet), the non-polar portion of Arg288 side chain (H3), Leu353 side chain (H6), and the side chain of Met364 (H7). These interactions can be seen in **Figure 9B**. The carbon tail of **4b** makes hydrophobic interactions with H6 and H7 which include those to the side chain of Met364, the side chain of Phe363 (H7), the side chain of Phe360 (H7), and the side chain of Leu353 (H6) as shown in **Figure 9C**. Given that we also produced a docked structure of **4b** bound to PPARγ that was in excellent agreement with our X-ray crystal structure, we hypothesized that further structural analysis of the other compounds could be carried out using docking techniques.

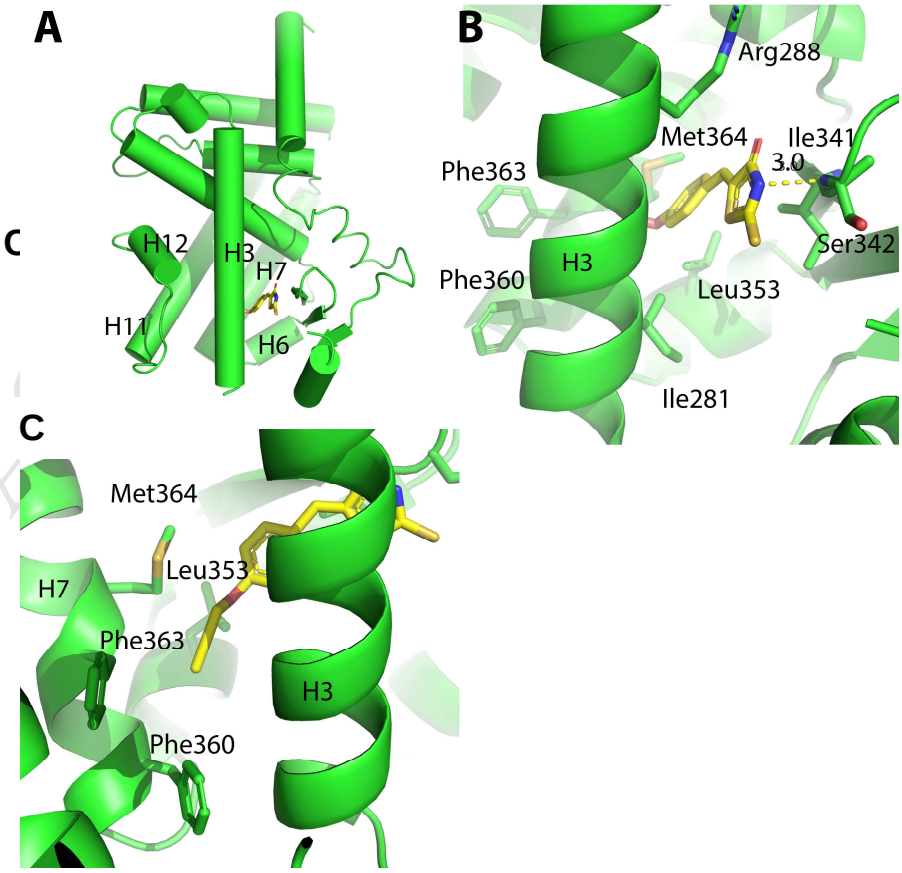

Figure 9. Binding mode of 4b to PPARγ as determined by X-ray crystallography (PDB accession code 6E5A). PPARγ is shown in green ribbons, compound **4b** is shown in yellow sticks, and residues of PPARγ within 3.5Å of the ligand are depicted as green sticks. **A)** Overview of the entire PPARγ LBD bound to **4b**. **B)** Interactions of **4b** with the beta-sheet and H3 region. **C)** Interactions of the carbon tail of **4b** with residues of the hydrophobic pocket formed by H7, and H3.

2.6. Molecular Modeling:

2.6.1. Docking of compounds 4b, 5b, 5g and 5e into COX-2 active site

The screening performance of COX-2 DEKOIS 2.0 benchmark set showed a good and non-random result with three docking tools (e.g., GOLD [ChemPLP], Glide [SP] and AutoDock Vina) [42]. Hence, we employed GOLD (ChemPLP) as scoring function for pose prediction purposes using PDB code of 1CX2 crystal structure for COX-2 docking. It has been reported that variation in molecular weight can cause obvious bias in docking performance especially when employing empirical scoring functions, since heavier molecules tend to produce superior scores [75,76]. Minimizing such bias would be of benefit in the context of correlating the docking scores of compounds with their biological *in vitro* activity values.

Due to variability in molecular weights of the test compounds and in order to eliminate this bias, score normalization strategy was applied by dividing the docking score by the number of heavy atoms (N) using different arithmetic weights (e.g., square root of N ($N^{1/2}$), cube root of N ($N^{1/3}$) and cube root of the squared N ($N^{2/3}$)) [77]. To select the most suitable normalization strategy, we evaluated the docking screening performance employing such strategies using COX-2 DEKOIS 2.0 benchmark set, and visualized the results using "pROC-Chemotype" plots **(Supplementary information Figures SM3-7)**. Besides, employing benchmarking would enable the effective detection of active ligands in a pool of their false positive decoys.

Since the screening performance results (based on pROC-AUC metric) were in the following order: $N^{1/3} > N^{1/2} > N^{2/3} >$ original score > N **(Supplementary information Figures SM3-7)**. Therefore, we employed ($N^{1/3}$) normalization scheme for our docking investigation on COX-2. We also used the same normalization scheme ($N^{1/3}$) for LOX docking experiments.

Interestingly, celecoxib and indomethacin displayed the highest and lowest docking scores with the synthesized compounds in-between, in both normalized and non-normalized panels. This correlates clearly with their *in vitro* activity against recombinant COX-2 enzyme, as seen in **Supplementary information Figures SM8**.

The normalized docking performance of all compounds seems to be comparable based on their mean values and standard deviation ranges, as shown in **Figure SM8B**. Interestingly, regarding the non-normalized docking fitness, the difference between the heaviest compound **6j** and the lightest one **4b** appeared to be significant since **4b** lies out of the standard deviation range of **6j** (**Figure SM8A**). However, after employing $N^{1/3}$ normalization, both **6j** and **4b** appeared comparable (**Figure SM8B**) which appeared to agree with their actual biological activities.

Additionally, docking of the compounds in the active sites of both COX-1 and COX-2 enzymes showed preference for COX-2 over COX-1. This was not surprising since the average molecular weights range of our compounds is 446.6 ±64.5 which is higher than average range of the diverse and representative COX-1 and COX-2 ligands reported in DEKOIS 2.0 benchmark sets (the average molecular weight of COX-1 and COX-2 in DEKOIS 2.0 benchmark set are 333.8 [± 62.97] and 373.6 [± 50.65], respectively) [42]. As well, it is well-recognized that COX-2 binding site is topologically larger than that of COX-1 and hence accommodates heavier ligands [78].

Since compounds **4b**, **5b**, **5e** and **5g** showed the highest activities in COX-2 and LOX binding assays as well as PPARγ translocation and functional reporter gene assays, we will focus on rationalizing their pose interactions in the binding sites of these targets.

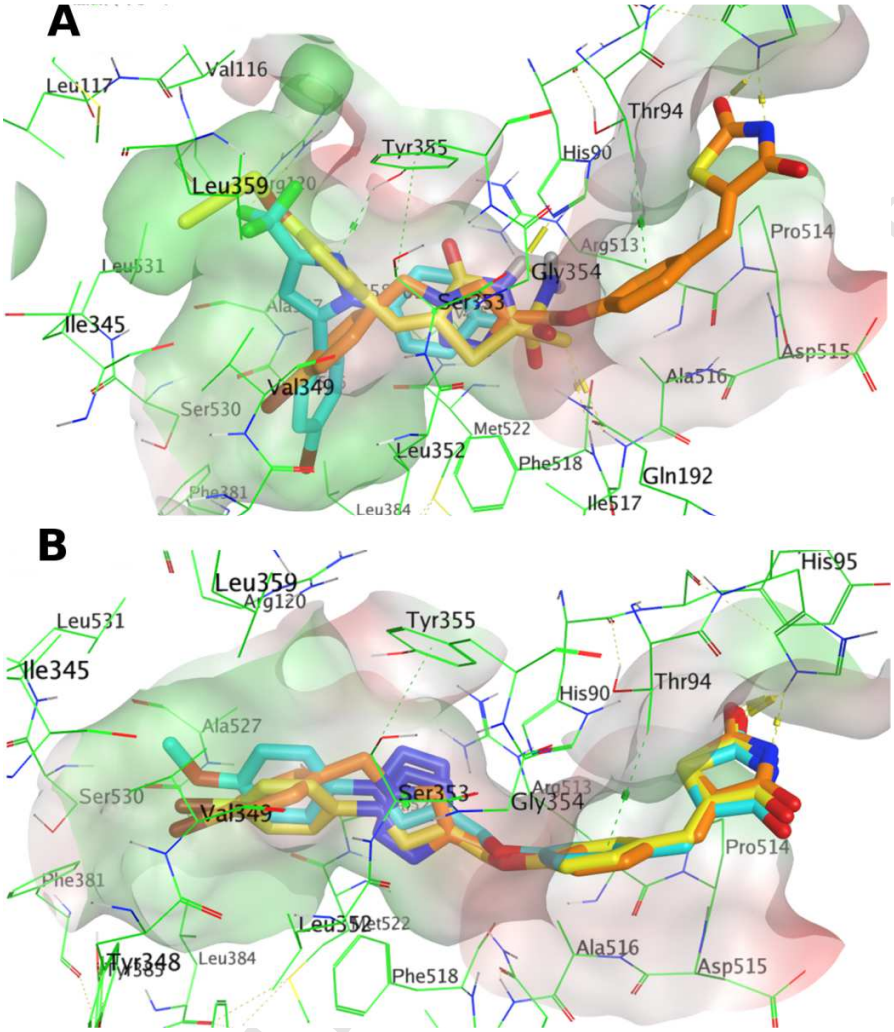

Figure 10. **(A)** Overlay of the docking poses of **4b** (yellow sticks), the co-crystallized ligand (cyan sticks) and **5b** (orange sticks) in the binding site of COX-2 (PDB: 1cx2). **(B)** Overlay of the docking poses of **5b** (orange sticks), **5g** (cyan sticks) and **5e** (yellow sticks) in the binding site of COX-2 (PDB: 1cx2). Polar and non-polar regions of the binding site were presented by red and green colored molecular surface, respectively. Dashed lines indicate favorable interactions. Non-polar hydrogen atoms were omitted for clarity.

The postulated binding pose of **4b** demonstrated hydrophobic and polar contacts, comprised by its phenoxy propargyl and rhodanine moieties, respectively (**Figure 10A**). The propargyl tail appeared to be packed deeply in the binding cleft formed by the side chains of Leu359, Val116, Ile345 and Arg120. Such interaction pattern resembled the favored hydrophobic contacts of the trifluoromethyl group of the co-crystallized selective COX-2 inhibitor (SC-558), albeit, with a deeper filling of the propargyl group towards the hydrophobic cleft aligned by Leu531.

The phenoxy group showed hydrophobic contacts with Tyr355 and Ala577. On the other hand, the rhodanine moiety appeared to act as a H-bonding donor to His90 via the imide group and reaches a favorable hydrophobic contact with the side chain of Ile517 via the thione group. This directed the rhodanine moiety towards the polar region of the binding site and overlaying on the sulfonamide group of SC-558.

The docking poses of **5b**, **5g** and **5e** showed comparable types of interactions in the binding site of COX-2 (**Figure 10B**). Their thiazolidinedionyl moieties acted as H-bonding acceptor for the side chain of His95 via the deprotonated imide and the carbonyl group at position number two in the ring.

Also, their aromatic phenoxy moieties appeared to demonstrate favorable hydrophobic interactions with the side chains of Thr94 and Ala516. Their triazolyl groups were packed between Ser353 and Val523. The lipophilic tail comprised terminal *p*-bromobenzyl, phenoxyphenyl and bromophenyl groups for **5b**, **5g** and **5e**, respectively, filled the hydrophobic region of the binding site and packed between the side chains of Val349, Leu352 and Ala527.

Generally, these postulated binding interactions of **4b** pose are obviously different than that of its congeneric analogues **5b**, **5g** and **5e**, where the latter poses showed superior scores due to more interactions and better pose accommodations. This observation is attributable to the fact that **4b** has dissimilar topological features (e.g., molecular weight and size) compared to the aforementioned 3 compounds. In addition, the large size of COX-2 binding site can accommodate different poses of a ligand.

2.6.2. Docking of compounds 4b, 5b, 5g and 5e into 15-LOX active site:

Again, the original docking fitness showed obvious fluctuations especially for the reference compounds NDGA and quercetin, and **4b**. Interestingly, when employing score normalization by ($N^{1/3}$), the docking fitness distribution appeared to be more homogenous, as seen in **Supplementary information Figures SM9**. This correlates better with the biological activity since almost all the compounds – including the reference compounds - lay within the same activity ranges.

The postulated binding pose of **4b** demonstrated mainly hydrophobic contacts in the binding site of 15-LOX (**Figure 11A**). The rhodanine moiety is packed between Gln590, Glu357, Ile418 and Ile593, Phe353. Also a postulated H-bonding interaction between the carbonyl group of the ring with Gln548 can be observed. The hydrophobic tail of **4b** comprising the phenoxy and propargyl groups packed between the backbone of Glu357, His361, His366, Asn401 and the side chain of Ile400.

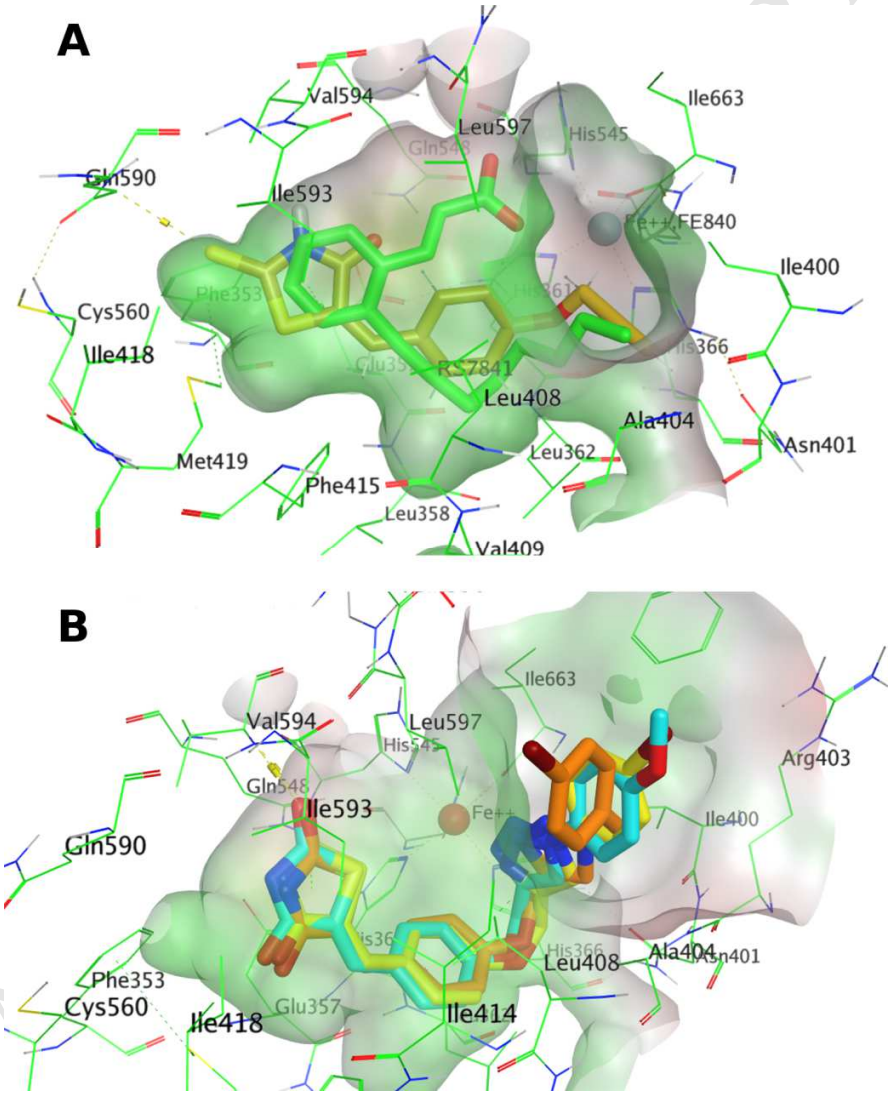

Figure 11. **(A)** Overlay of the docking poses of 4b (gold sticks) and the co-crystallized ligand (green sticks) in the binding site of 15-LOX (PDB: 1lox). **(B)** Overlay of the docking poses of 5b (orange sticks), 5g (cyan sticks) and 5e (yellow sticks) in the binding site of 15-LOX (PDB: 1lox). Polar and non-polar regions of the binding site were presented by red and green colored molecular surface, respectively.

Dashed lines indicate favorable interactions. Non-polar hydrogen atoms were omitted for clarity.

Again, the postulated binding poses of **5b**, **5g** and **5e** showed comparable types of interactions in the binding site of 15-LOX mostly by hydrophobic and Van der Waal types of interactions (**Figure 11B**). However, their thiazolidinedione moieties acted as H-bonding acceptor for the amidic backbone of Val594 via the carbonyl group at position two in the ring. Their aromatic phenoxy moieties packed between the hydrophobic side chains of Val409, Leu362, Leu358 and Phe415 indicating favorable hydrophobic interactions. Furthermore, their triazolyl groups filled the space formed by the side chain of Ile400, Leu408 and Leu597. The lipophilic terminals of p-bromobenzyl, phenoxyphenyl and bromophenyl groups for **5b**, **5g** and **5e**, respectively, packed between the side chains of Leu597, Phe175, Ileu414 and the backbone of Ala404 and Arg403; nevertheless, the bromo and methoxy groups appeared to be solvent exposed. No metal chelation was observed for postulated binding poses of **4b**, **5b**, **5g** and **5e**.

2.7. *In silico* prediction of physicochemical properties, drug-likeness, pharmacokinetic profile and ligand efficiency metrics:

In the present work, physicochemical and pharmacokinetic parameters of the most active compounds **4b**, **5b**, **5e** and **5g** were calculated using Molinspiration [79], Molsoft [80], Pre-ADMET [81] and Data warrior [82] software.

Results presented in **Supplementary Information Table SM4** showed that the four compounds obeyed Lipinski's rule, with LogP values between 2.04 and 3.69 (<5), MW ranging between 275 and 471 (<500) together with number of HBA and HBD of 3-8 (<10) and 1 (<5), respectively. Hence, these compounds should not demonstrate a problem regarding oral absorption. Moreover, the compounds showed NROTB values of 3-6 (<10) and TPSA values of 42.10-99.12 $Å^2$ (<140 $Å^2$), indicating their potential to be transported through biological membranes.

Molsoft software was used to calculate the solubility and drug-likeness model score. Although, the drug-likeness predicted values for the test compounds ranged between -0.73 and -0.1, yet they passed the solubility cut-off limit with values of 0.03-0.98

mg/L (more than 0.0001 mg/L). Since aqueous solubility is known to influence both absorption and distribution characteristics remarkably, we predict that these compounds can behave as drug-like.

Furthermore, *in silico* prediction of the pharmacokinetic parameters was carried out using Pre-ADMET software. Results of the predicted ADME parameters are recorded in **Table SM4**. Medium cell permeability in the Caco-2 cell model was predicted for the four compounds with values between 12.86 and 40.82 nm/s. They also can be regarded as well-absorbed molecules due to high human intestinal absorption values (around 97%). Moreover, they showed low BBB penetrability (0.03-0.1) and high binding ability to human plasma proteins (91.83-100%). As well, they were non-inhibitors of CYP2D6 enzyme and thus interactions with CYP2D6 inducers and/or inhibitors should not present a problem.

Endeavors to incorporate physicochemical properties (i.e. molecular weight, polar surface area, lipophilicity and others), together with potency into a quantitative and numerical framework have recently materialized into ligand efficiency indices. These are composite and easy-to-follow prognosticators that were formulated to help increase the robustness of the drug discovery process and provide more favorable outcomes. They blend potency, lipophilicity and heavy atom count, thus guiding the lead optimization process along the preclinical drug discovery path [83].

Hence, prospective assessment of the quality of the most active compounds as potential hits or leads was achieved by application of these metrics, namely; Ligand efficiency (LE), lipophilic ligand efficiency (LLE) and ligand efficiency-dependent lipophilicity index (LELP) using Data warrior software.

LE is a link between drug potency and its molecular size in the form of heavy (non-hydrogen) atom count. Regarding both COX-2 and 15-LOX inhibitory activities, LE values of the four compounds ranged from 0.25 to 0.53 which adhere to the accepted minimum LE for lead compounds (in the range of 0.3) or > 0.3 for drug candidates [84,85].

LLE correlates potency to lipophilicity. With the exception of **5b** and **5e** anti-LOX activity (LLE = 2.55 and 2.94, respectively), LLE values for both enzymatic

inhibitory activities, shown in **Table SM4**, ranged from 3.86 to 5.82, which comply with the optimum cut-off values for lead compounds (≥ 3) or drug candidates (≥ 5) [85].

LELP is considered as a combined scoring function and hence with greater predictive power as it relates both molecular size and lipophilicity to potency. In addition, unlike LE and LLE, LELP has been reported to have the ability to differentiate between marketed drugs and unsuccessful leads not to mention its high correlation with pharmacokinetic profile and safety [86].

Interestingly, both COX and LOX inhibition afforded LELP values that fulfilled the accepted limits for leads (≤7.5) or marketed drugs (<10) since their values ranged from 2.09 to 9.23 [85]. This is in contrast to **5b**, which showed LELP value of 10.84 for LOX inhibition, which slightly deviated from the value reported for drug candidates.

Enlightened by the aforementioned drug-likeness, ADME and ligand efficiency predictions, these compounds demonstrated their appropriateness for further lead optimization studies.

3. Conclusion:

In this study, for the first time, we have described the design of novel triazolyl-thiazolidinedione/rhodanine hybrids as potential simultaneous COX-2/LOX inhibitors and PPARγ partial agonists. We challenged our design with pre-synthetic docking experiments on PPARγ using three docking software, which showed encouraging docking scores, interactions with key amino acids and comparable orientation of the docked compounds with respect to the co-crystallized ligand rosiglitazone. Most of the synthesized hybrids showed micromolar inhibitory activities towards COX-2 and 15-LOX in *in vitro* assays. *In vitro* glucose uptake assay identified compounds **4b**, **5e** as stronger glucose uptake inducers than pioglitazone in the presence and absence of insulin, and compounds **5b**, **5g** as equal or higher glucose uptake inducers in an insulin-independent fashion, which raises the possibility of selective targeting of PPARγ signaling pathways. Immunohistochemical analysis of ligand-stimulated

PPARγ nuclear localization confirmed the ability of compounds **4b**, **5b**, **5e** and **5g** to induce PPARγ nuclear translocation, similar to pioglitazone. Moreover, PPARγ functional reporter gene assay confirmed the partial agonistic activity of the latter 4 compounds towards PPARγ. The same 4 compounds were capable to inhibit monocyte to macrophage differentiation, which is a pivotal and early step in inflammatory response. As expected, the most potent 15-LOX inhibitors **4b**, **5e** & **5g** reduced inflammatory cytokine production and arachidonate metabolism in human macrophage model challenged by LPS. Over and above, compound **4b** demonstrated a statistically significant higher potency compared to celecoxib in formalin-induced rat paw edema assay. While, compounds **5b, 5e and 5g** showed equivalent inhibitory effect to the reference drugs. X-ray crystallography of compound **4b** with PPARγ showed its binding outside AF2 part of LBD, which is the part responsible for the full activation of PPARγ and hence complete recruitment of downstream signaling molecules. Instead, it managed to pursue other hydrophobic interactions with residues in H3, H6 and H7 parts of LBD via its phenyl ring and propargyl tail. Also, a key hydrogen bonding interaction with Ser342 in beta sheet was observed. We believe that the presence of only one carbonyl group in rhodanine part of **4b** probably changed its ability to bind to AF2 and hence might be partly responsible for its partial agonistic activity. Another part of the partial agonistic activity could be attributed to the hydrophobic interactions, especially those of the propargylic tail. Molecular docking experiments of compounds **4b**, **5b**, **5e** and **5g** on COX-2 and 15-LOX showed perfect fitting in the binding pocket and noticeable interactions with key amino acids. The docking scores after appropriate normalization correlated successfully with the *in vitro* biological data. Appropriate normalization was granted by using COX-2 DEKOIS 2 benchmark set. Moreover, drug-likeness assessment via Molinspiration, Molsoft, Pre-ADMET and Data warrior software elucidated their full compliance with Lipinski's rule, favorable physicochemical properties and convenient predicted pharmacokinetic parameters. Over and above, ligand efficiency metrics for compounds **4b**, **5b** and **5e** were calculated and they indicated that these 3 compounds represent promising hits/leads to pursue as potential simultaneous COX-2/LOX inhibitors and PPARγ partial agonists for management of inflammatory disorders. We

think that compounds **4b**, **5b** and **5e** will be insightful additions to the contemporary drug design programs directed towards inflammatory disorders with potential links to metabolic diseases.

Ackowledgements:

X-ray crystallography part of this research was undertaken on the MX1 beamline at the Australian Synchrotron, part of ANSTO. Also, all authors acknowledge Prof. F Boeckler, Lab for Molecular Design and Pharmaceutical Biophysics, Eberhard Karls University Tuebingen, Germany, for granting access to some computational tools. This study was partially supported by MPP grant # 320148 from the Faculty of Medicine at the American University of Beirut and was presented in preliminary form at Experimental Biology 2018.

4. Experimental:

4.1. Chemistry:

All chemicals were purchased from commercial suppliers and used without further purification. Melting points were recorded on electrotherm capillary tube Stuart melting point apparatus SMP10 and are all uncorrected. Follow up of the reactions' rates were performed by thin-layer chromatography (TLC) on silica gel-precoated aluminum sheets (Type 60 GF254; Merck; Germany) and the spots were visualized by exposure to iodine vapors or UV-lamp at λ 254nm for few seconds. Infrared spectra (IR) were recorded using KBr discs on a Shimadzu IR 435 spectrophotometer, Faculty of Pharmacy, Cairo University. Nuclear magnetic resonance (^{1}H NMR and ^{13}C NMR) spectra were recorded on a Jeol spectrometer (500 MHz) at the Microanalytical Unit, Faculty of Science, University of Alexandria or on a Bruker (400 MHz) spectrophotometer, Faculty of Pharmacy, Cairo University using deuterated Dimethylsulfoxide (DMSO-d_6) as solvent. The data were recorded as chemical shifts expressed in δ (ppm) relative to Tetramethylsilane (TMS) as internal standard. Signal splitting are expressed by the following abbreviations: s = singlet, d = doublet, t = triplet, q = quartet and m = multiplet. The purity of the new compounds was checked

by elemental analyses (C, H, N and S), conducted on FLASH 2000 CHNS/O analyzer, Thermo Scientific at the regional center for mycology and biotechnology (RCMB), Al-Azhar University. In addition, new compounds were found to be ≥95% pure by reversed phase HPLC analysis using Agilent 1260 infinity HPLC equipped with G1311B Quaternary pump, G1329 injector and G 1315D DAD Vl detector. A G1316A C18 column (4.6 x 150 mm) was used. An injection volume of 0.5 ml (DMF and phosphate buffer pH 5 1:1), a flow rate of 1 mL/min and an isocratic elution of acetonitrile in water (1:1) were applied. Analyses were monitored at 254 nm wavelength. The preparation of appropriate azides [87,88], propargyl derivative **2** [89] and aldehydes **3(a-h)** [90] were performed according to reported procedures.

4.1.1. Knoevenagel condensation procedure for compounds 4(a,b), 5(a-h) and 6(a-h) :

A mixture of the appropriate aldehyde (**2** or **3**(**a-h**)) and thiazolidine-2,4-dione / rhodanine (1mmole) with catalytic quantity of piperidine (10 mol%) in absolute ethanol was refluxed for 12 hours. After cooling to room temperature overnight, the precipitated compound was filtered, washed with ice-cooled ethanol and dried. The solid was crystallized from ethanol or ethanol/DMF to obtain the appropriate solid products.

(*Z*)-5-(4-(prop-2-yn-1-yloxy)benzylidene)thiazolidine-2,4-dione **(4a)**

Yield 74%. m.p. 216-218 °C. ^{1}H NMR (400 MHz, DMSO-d_6): δ 12.51 (s, 1H, NH, D_2O exchangeable), 7.73 (s, 1H, benzylidene-CH), 7.55 (d, *J* = 8.84 Hz, 2H, benzylidene- $C_{2,6}$-H), 7.13 (d, *J* = 8.84 Hz, 2H, benzylidene- $C_{3,5}$-H), 4.88 (d, *J* = 2.32 Hz, 2H, OCH_2), 3.61 (t, *J* = 2.32 Hz, 1H, C≡CH). ^{13}C NMR (100 MHz, DMSO-d_6): δ 168.4, 167.9, 159.3, 132.4, 132.1, 126.6, 121.3, 116.1, 79.2, 79.1, 56.2. IR (KBr): cm^{-1} 3275.13 (C≡C<u>H</u>), 3097.68 (NH), 2376.30-2322.29 (C≡C), 1732.08 (C=O), 1678.07 (amide C=O), 1639.49 (C=N), 1589.34 (C=C), 1257.59 and 1022.27 (C-O-C), (C-S-C). Anal. Calcd (%) for $C_{13}H_9NO_3S$ (259.28): C, 60.22; H, 3.50; N, 5.40; S, 12.37. Found C, 60.48; H, 3.64; N, 5.61; S, 12.52. HPLC / DAD: Retention time 4.93 min.

(*Z*)-5-(4-(prop-2-yn-1-yloxy)benzylidene)-2-thioxothiazolidin-4-one **(4b)**

Yield 69%. m.p. 226-228 °C. ^{1}H NMR (400 MHz, DMSO-d_6): δ 13.76 (s, 1H, NH, D_2O exchangeable), 7.60 (s, 1H, benzylidene-CH), 7.57 (d, *J* = 8.84 Hz, 2H,

benzylidene- $C_{2,6}$-H), 7.15 (d, *J* = 8.84 Hz, 2H, benzylidene- $C_{3,5}$-H), 4.90 (d, *J* = 2.32 Hz, 2H, OCH_2), 3.63 (t, *J* = 2.32 Hz, 1H, C≡CH). ^{13}C NMR (100 MHz, DMSO-d_6): δ 196.1, 170.2, 159.6, 133.0, 132.0, 126.7, 123.4, 116.3, 79.2, 79.1, 56.2. IR (KBr): cm^{-1} 3255.84 (C≡C<u>H</u>), 3001.24 (NH), 2376.30-2322.29 (C≡C), 1685.79 (amide C=O), 1640 (C=N), 1581.63 (C=C), 1246.02 and 1068.56 (C-O-C), (C-S-C). Anal. Calcd (%) for $C_{13}H_9NO_2S_2$ (275.34): C, 56.71; H, 3.29; N, 5.09; S, 23.29. Found C, 57.04; H, 3.18; N, 5.37; S, 23.44. HPLC / DAD: Retention time 9.5 min.

(*Z*)-5-(4-((1-benzyl-1*H*-1,2,3-triazol-4-yl)methoxy)benzylidene)thiazolidine-2,4-dione **(5a)**

Yield 83%. m.p. 178-180 °C. ^{1}H NMR (500 MHz, DMSO-d_6): δ 12.49 (s, 1H, NH, D_2O exchangeable), 8.29 (s, 1H, triazole-C_5-H), 7.73 (s, 1H, benzylidene-CH),7.53 (d, *J* = 8.4 Hz, 2H, benzylidene-$C_{2,6}$-H), 7.37-7.28 (m, 5H, phenyl-$_{C1,2,3,4,5}$-H), 7.17 (d, *J* = 8.4 Hz, 2H, benzylidene- $C_{3,5}$-H), 5.59 (s, 2H, NCH_2), 5.20 (s, 2H, OCH_2). ^{13}C NMR (125 MHz, DMSO-d_6): δ 160.2, 143.0, 132.6, 126.4, 121.1, 116.2, 61.9, 53.4. IR (KBr): cm^{-1} 3140.11 (NH), 1743.65 (C=O), 1678.07 (amide C=O), 1635 (C=N), 1597.06 (C=C), 1249.87 and 1040 (C-O-C), (C-S-C). Anal. Calcd (%) for $C_{20}H_{16}N_4O_3S$ (392.43): C, 61.21; H, 4.11; N, 14.28; S, 8.17. Found C, 61.47; H, 4.24; N, 14.59; S, 8.24. HPLC / DAD: Retention time 4.29 min.

(*Z*)-5-(4-((1-(4-bromobenzyl)-1*H*-1,2,3-triazol-4-yl)methoxy)benzylidene) thiazolidine-2,4-dione **(5b)**

Yield 86%. m.p. 182-184 °C. ^{1}H NMR (500 MHz, DMSO-d_6): δ 12.45 (s, 1H, NH, D_2O exchangeable), 8.29 (s, 1H, triazole-C_5-H), 7.73 (s, 1H, benzylidene-CH), 7.37-7.28 (m, 4H, 4-bromophenyl-$C_{2,6}$-H and benzylidene-$C_{3,5}$-H), 7.24 (d, *J* = 8.4 Hz, 2H, benzylidene-$C_{2,6}$-H), 7.17 (d, *J* = 8.4 Hz, 2H, 4-bromophenyl- $C_{3,5}$-H), 5.58 (s, 2H, NCH_2), 5.20 (s, 2H, OCH_2). ^{13}C NMR (125 MHz, DMSO-d_6): δ 168.5, 168.1, 160.2, 143.1, 132.6, 126.4, 122.0, 116.2, 61.8, 52.6. IR (KBr): cm^{-1} 3136.25 (NH), 1735.93 (C=O), 1685.79 (amide C=O), 1635 (C=N), 1585.49 (C=C), 1257.59 and 1053.13 (C-O-C), (C-S-C). Anal. Calcd (%) for $C_{20}H_{15}BrN_4O_3S$ (471.33): C, 50.97; H, 3.21; N, 11.89; S, 6.80. Found C, 51.24; H, 3.39; N, 11.75; S, 6.71. HPLC / DAD: Retention time 7.83 min.

(*Z*)-5-(4-((1-phenyl-1*H*-1,2,3-triazol-4-yl)methoxy)benzylidene)thiazolidine-2,4-dione **(5c)**

Yield 85%. m.p. 262-264 °C. ^{1}H NMR (400 MHz, DMSO-d_6): δ 12.53 (s, 1H, NH, D_2O exchangeable), 8.99 (s, 1H, triazole-C_5-H), 7.92 (d, J = 7.8 Hz, 2H, phenyl-$C_{2,6}$-H), 7.77 (s, 1H, benzylidene-CH), 7.49-7.64 (m, 5H, benzylidene- $C_{2,6}$-H and phenyl-$C_{3,4,5}$-H), 7.26 (d, J = 8.72 Hz, 2H, benzylidene- $C_{3,5}$-H), 5.34 (s, 2H, OCH_2). ^{13}C NMR (100 MHz, DMSO-d_6): δ 168.5, 160.1, 143.9, 137.0, 132.6, 132.2, 130.4, 129.3, 126.5, 123.6, 120.7, 116.1, 61.7. IR (KBr): cm^{-1} 3151.69 (NH), 1739.79 (C=O), 1693.50 (amide C=O), 1640 (C=N), 1597.06 (C=C), 1253.73 and 1053.13 (C-O-C), (C-S-C). Anal. Calcd (%) for $C_{19}H_{14}N_4O_3S$ (378.41): C, 60.31; H, 3.73; N, 14.81; S, 8.47. Found C, 59.96; H, 3.88; N, 15.07; S, 8.65. HPLC / DAD: Retention time 5.99 min.

(*Z*)-5-(4-((1-(4-chlorophenyl)-1*H*-1,2,3-triazol-4-yl)methoxy)benzylidene) thiazolidine-2,4-dione **(5d)**

Yield 80%. m.p. 243-245 °C. ^{1}H NMR (400 MHz, DMSO-d_6): δ 12.54 (s, 1H, NH, D_2O exchangeable), 9.02 (s, 1H, triazole-C_5-H), 7.26-7.97 (m, 9H, 4-chlorophenyl-$C_{2,3,5,6}$-H, benzylidene- $C_{2,3,5,6}$-H and benzylidene-CH), 5.35 (s, 2H, OCH_2). ^{13}C NMR (100 MHz, DMSO-d_6): δ 168.5, 160.1, 144.0, 135.8, 133.6, 132.6, 132.2, 130.3, 126.5, 123.6, 122.3, 116.1, 61.7. IR (KBr): cm^{-1} 3159.40 (NH), 1732.08 (C=O), 1693.5 (amide C=O), 1640 (C=N), 1589.34 (C=C), 1265.30 and 1033.85 (C-O-C), (C-S-C). Anal. Calcd (%) for $C_{19}H_{13}ClN_4O_3S$ (412.85): C, 55.28; H, 3.17; N, 13.57; S, 7.77. Found C, 55.60; H, 3.08; N, 13.81; S, 7.59. HPLC / DAD: Retention time 10.51 min.

(*Z*)-5-(4-((1-(4-bromophenyl)-1*H*-1,2,3-triazol-4-yl)methoxy)benzylidene)thiazolidine-2,4-dione **(5e)**

Yield 88%. m.p. 143-145 °C. ^{1}H NMR (400 MHz, DMSO-d_6): δ 12.52 (s, 1H, NH, D_2O exchangeable), 8.99 (s, 1H, triazole-C_5-H), 7.88 (d, J = 8.72 Hz, 2H, 4-bromophenyl-$C_{3,5}$-H), 7.78 (d, J = 8.72 Hz, 2H, 4-bromophenyl-$C_{2,6}$-H), 7.75 (s, 1H, benzylidene-CH), 7.56 (d, J = 8.56 Hz, 2H, benzylidene- $C_{2,6}$-H), 7.23 (d, J = 8.56 Hz, 2H, benzylidene- $C_{3,5}$-H), 5.33 (s, 2H, OCH_2). ^{13}C NMR (100 MHz, DMSO-d_6): δ 168.5, 160.1, 144.1, 136.2, 133.2, 132.6, 132.2, 126.5, 123.5, 122.5, 121.9, 116.1, 61.7. IR (KBr): cm^{-1} 3143.97 (NH), 1728.22 (C=O), 1670.35 (amide C=O), 1640 (C=N), 1585.49 (C=C), 1253.73 and 1072.42 (C-O-C), (C-S-C). Anal. Calcd (%) for $C_{19}H_{13}BrN_4O_3S$ (457.30): C, 49.90; H, 2.87; N, 12.25; S, 7.01. Found C, 49.76; H, 2.91; N, 12.47; S, 7.14. HPLC / DAD: Retention time 11.90 min.

(*Z*)-5-(4-((1-(p-tolyl)-1*H*-1,2,3-triazol-4-yl)methoxy)benzylidene)thiazolidine-2,4-dione **(5f)**

Yield 90%. m.p. 248-250 °C. ^{1}H NMR (400 MHz, DMSO-d_6): δ 12.55 (s, 1H, NH, D_2O exchangeable), 8.92 (s, 1H, triazole-C_5-H), 7.25-7.78 (m, 9H, p-tolyl -$C_{2,3,5,6}$-H, benzylidene- $C_{2,3,5,6}$-H and benzylidene-CH), 5.32 (s, 2H, OCH_2), 2.38 (s, 3H, CH_3). ^{13}C NMR (100 MHz, DMSO-d_6): δ 168.5, 168.0, 160.1, 143.7, 138.9, 134.8, 132.5, 132.1, 130.7, 126.4, 123.4, 121.2, 120.5, 116.1, 61.7, 21.0. IR (KBr): cm^{-1} 3147.83 (NH), 1724.36 (C=O), 1666.50 (amide C=O),1630 (C=N), 1589.34 (C=C), 1253.73 and 1026.13 (C-O-C), (C-S-C). Anal. Calcd (%) for $C_{20}H_{16}N_4O_3S$ (392.43): C, 61.21; H, 4.11; N, 14.28; S, 8.17. Found C, 61.48; H, 4.24; N, 14.70; S, 8.34. HPLC / DAD: Retention time 8.78 min.

(*Z*)-5-(4-((1-(4-methoxyphenyl)-1*H*-1,2,3-triazol-4-yl)methoxy)benzylidene) thiazolidine -2,4-dione **(5g)**

Yield 86%. m.p. 248-250 °C. ^{1}H NMR (400 MHz, DMSO-d_6): δ 12.39 (s, 1H, NH, D_2O exchangeable), 8.87 (s, 1H, triazole-C_5-H), 7.82 (d, *J* = 5.6, 2H, benzylidene-$C_{2,6}$-H), 7.76 (s, 1H, benzylidene-CH), 7.58 (d, *J* = 5.28 Hz, 2H, 4-methoxyphenyl-$C_{2,6}$-H), 7.26 (d, *J* = 5.28 Hz, 2H, 4-methoxyphenyl- $C_{3,5}$-H), 7.14 (d, *J* = 5.6 Hz, 2H, benzylidene- $C_{3,5}$-H), 5.32 (s, 2H, OCH_2), 3.84 (s, 3H, OCH_3). ^{13}C NMR (100 MHz, DMSO-d_6): δ 168.6, 168.4, 160.1, 159.8, 143.6, 132.5, 131.9, 130.4, 126.5, 123.5, 122.3, 121.4, 116.1, 115.4, 61.8, 56.0. IR (KBr): cm^{-1} 3116.97 (NH), 1739.79 (C=O), 1685.79 (amide C=O), 1635 (C=N), 1589.34 (C=C), 1249.87 and 1022 (C-O-C), (C-S-C). Anal. Calcd (%) for $C_{20}H_{16}N_4O_4S$ (408.43): C, 58.82; H, 3.95; N, 13.72; S, 7.85. Found C, 59.05; H, 4.02; N, 14.07; S, 7.59. HPLC / DAD: Retention time 6.00 min.

(*Z*)-4-(4-((4-((2,4-dioxothiazolidin-5-ylidene)methyl)phenoxy)methyl)-1*H*-1,2,3-triazol-1-yl)benzoic acid **(5h)**

Yield 82%. m.p. >300 °C. ^{1}H NMR (400 MHz, DMSO-d_6): δ 13.28 (s, 1H, COOH, D_2O exchangeable), 12.59 (s, 1H, NH, D_2O exchangeable), 9.15 (s, 1H, triazole-C_5-H), 8.20 (d, *J* = 8.6 Hz, 2H, 4-carboxyphenyl-$C_{3,5}$-H), 8.13 (d, *J* = 8.6 Hz, 2H, 4-carboxyphenyl- $C_{2,6}$-H), 7.82 (s, 1H, benzylidene-CH), 7.64 (d, *J* = 8.68 Hz, 2H, benzylidene- $C_{2,6}$-H), 7.30 (d, *J* = 8.68 Hz, 2H, benzylidene-$C_{3,5}$-H), 5.41 (s, 2H, OCH_2). ^{13}C NMR (100 MHz, DMSO-d_6): δ 168.4, 167.9, 166.8, 160.1, 144.2, 139.9, 132.6, 132.2, 131.6, 131.2, 126.4, 123.7, 121.1, 120.4, 116.1, 61.7. IR (KBr): cm^{-1} 3367.71-2962.66 (OH), 3143.97 (NH), 1739.79 (C=O), 1670.35 (amide C=O), 1610

(C=N), 1589.34 (C=C), 1253.73 and 1026.13 (C-O-C), (C-S-C). Anal. Calcd (%) for $C_{20}H_{14}N_4O_5S$ (422.42): C, 56.87; H, 3.34; N, 13.26; S, 7.59. Found C, 57.21; H, 3.50; N, 12.98; S, 7.81. HPLC / DAD: Retention time 2.67 min.

(*Z*)-5-(4-((1-benzyl-1*H*-1,2,3-triazol-4-yl)methoxy)benzylidene)-2-thioxothiazolidin-4-one **(6a)**

Yield 80%. m.p. 186-188 °C. ^{1}H NMR (400 MHz, DMSO-d_6): δ 13.75 (s, 1H, NH, D_2O exchangeable), 8.32 (s, 1H, triazole-C_5-H), 7.62 (s, 1H, benzylidene-CH), 7.58 (d, *J* = 8.84 Hz, 2H, benzylidene- $C_{2,6}$-H), 7.32-7.40 (m, 5H, benzyl-Hs), 7.22 (d, *J* = 8.84 Hz, 2H, benzylidene-$C_{3,5}$-H), 5.62 (s, 2H, benzyl-CH_2), 5.25 (s, 2H, OCH_2). ^{13}C NMR (100 MHz, DMSO-d_6): δ 196.1, 170.1, 160.5, 142.9, 136.4, 133.1, 132.2, 129.3, 128.7, 128.4, 126.3, 125.4, 123.1, 116.3, 61.8, 53.3. IR (KBr): cm^{-1} 3136.25 (NH), 1693.50 (C=O), 1640(C=N), 1585.49 (C=C), 1261.45, 1172.72, and 1053.13 (C-O-C), (C=S) and (C-S-C). Anal. Calcd (%) for $C_{20}H_{16}N_4O_2S_2$ (408.49): C, 58.81; H, 3.95; N, 13.72; S, 15.70. Found C, 59.04; H, 3.88; N, 13.98; S, 15.93. HPLC / DAD: Retention time 9.44 min.

(*Z*)-5-(4-((1-(4-bromobenzyl)-1*H*-1,2,3-triazol-4-yl)methoxy)benzylidene)-2-thioxothiazolidin-4-one **(6b)**

Yield 81%. m.p. 138-140 °C. ^{1}H NMR (400 MHz, DMSO-d_6): δ 13.75 (s, 1H, NH, D_2O exchangeable), 8.33 (s, 1H, triazole-C_5-H), 7.62 (s, 1H, benzylidene-CH), 7.57-7.59 (m, 4H, 4-bromobenzyl-$C_{3,5}$-H and benzylidene-$C_{2,6}$-H), 7.28 (d, *J* = 7.88 Hz, 2H, 4-bromobenzyl-$C_{2,6}$-H), 7.21 (d, *J* = 8.32 Hz, 2H, benzylidene-$C_{3,5}$-H), 5.62 (s, 2H, benzyl-CH_2), 5.25 (s, 2H, OCH_2). ^{13}C NMR (100 MHz, DMSO-d_6): δ 196.1, 170.2, 160.5, 143.0, 135.8, 133.1, 132.2, 131.8, 130.7, 126.3, 125.5, 123.2, 121.9, 116.3, 61.8, 52.6. IR (KBr): cm^{-1} 3147.83 (NH), 1708.93 (C=O), 1620 (C=N), 1589.34 (C=C), 1242.16, 1172.72, and 1049.28 (C-O-C), (C=S) and (C-S-C). Anal. Calcd (%) for $C_{20}H_{15}BrN_4O_2S_2$ (487.39): C, 49.29; H, 3.10; N, 11.50; S, 13.16. Found C, 49.01; H, 3.24; N, 11.78; S, 13.49. HPLC / DAD: Retention time 15.17 min.

(*Z*)-5-(4-((1-phenyl-1*H*-1,2,3-triazol-4-yl)methoxy)benzylidene)-2-thioxothiazolidin-4-one **(6c)**

Yield 84%. m.p. 228-230 °C. ^{1}H NMR (400 MHz, DMSO-d_6): δ 13.70 (s, 1H, NH, D_2O exchangeable), 8.98 (s, 1H, triazole-C_5-H), 7.92 (d, *J* = 7.88 Hz, 2H,

benzylidene- $C_{2,6}$-H), 7.48-7.63 (m, 6H, benzylidene-CH and phenyl-Hs), 7.22-7.27 (m, 2H, benzylidene- $C_{3,5}$-H), 5.34 (s, 2H, OCH_2). ^{13}C NMR (100 MHz, DMSO-d_6): δ 196.4, 173.7, 160.3, 143.8, 137.0, 133.1, 131.7, 130.4, 129.9, 129.3, 126.6, 123.5, 120.7, 116.2, 61.7. IR (KBr): cm^{-1} 3132.40 (NH), 1708.93 (C=O), 1625 (C=N), 1589.34 (C=C), 1242.16,1168.86, and 1030 (C-O-C), (C=S) and (C-S-C). Anal. Calcd (%) for $C_{19}H_{14}N_4O_2S_2$ (394.47): C, 57.85; H, 3.58; N, 14.20; S, 16.25. Found C, 58.07; H, 3.65; N, 14.53; S, 16.48. HPLC / DAD: Retention time 11.45 min.

(*Z*)-5-(4-((1-(4-chlorophenyl)-1*H*-1,2,3-triazol-4-yl)methoxy)benzylidene)-2-thioxothiazolidin-4-one **(6d)**

Yield 92%. m.p. 268-270 °C. ^{1}H NMR (400 MHz, DMSO-d_6): δ 13.70 (s, 1H, NH, D_2O exchangeable), 9.00 (s, 1H, triazole-C_5-H), 7.96 (d, *J* = 8.72 Hz, 2H, 4-chlorophenyl-$C_{2,6}$-H), 7.68 (d, *J* = 8.72 Hz, 2H, 4-chlorophenyl-$C_{3,5}$-H), 7.58-7.60 (m, 3H, benzylidene- $C_{2,6}$-H and benzylidene-CH), 7.26 (d, *J* = 8.64 Hz, 2H, benzylidene-$C_{3,5}$-H), 5.34 (s, 2H, OCH_2). ^{13}C NMR (100 MHz, DMSO-d_6): δ 196.3, 170.6, 160.3, 144.1, 135.8, 133.6, 133.1, 131.8, 130.4, 126.5, 123.6, 123.5, 122.4, 116.3, 61.7. IR (KBr): cm^{-1} 3147.83 (NH), 1708.93 (C=O), 1620 (C=N), 1589.34 (C=C), 1238.30, 1168.86 and 1025 (C-O-C), (C=S) and (C-S-C). Anal. Calcd (%) for $C_{19}H_{13}ClN_4O_2S_2$ (428.91): C, 53.21; H, 3.06; N, 13.06; S, 14.95. Found C, 53.59; H, 3.19; N, 12.89; S, 15.01. HPLC / DAD: Retention time 8.33 min.

(*Z*)-5-(4-((1-(4-bromophenyl)-1*H*-1,2,3-triazol-4-yl)methoxy)benzylidene)-2-thioxothiazolidin-4-one **(6e)**

Yield 89%. m.p. 271-273 °C. ^{1}H NMR (400 MHz, DMSO-d_6): δ 13.78 (s, 1H, NH, D_2O exchangeable), 9.01 (s, 1H, triazole-C_5-H), 7.90 (d, *J* = 11.48 Hz, 2H, 4-bromophenyl-$C_{3,5}$-H), 7.81 (d, *J* = 11.48 Hz, 2H, 4-bromophenyl-$C_{2,6}$-H), 7.62 (s, 1H, benzylidene-CH), 7.59 (d, *J* = 8.84 Hz, 2H, benzylidene- $C_{2,6}$-H), 7.26 (d, *J* = 8.84 Hz, 2H, benzylidene- $C_{3,5}$-H), 5.35 (s, 2H, OCH_2). ^{13}C NMR (100 MHz, DMSO-d_6): δ 196.1, 170.1, 160.4, 144.0, 136.2, 133.3, 133.1, 132.1, 126.4, 123.6, 123.2, 122.6, 122.0, 116.3, 61.7. IR (KBr): cm^{-1} 3143.97 (NH), 1716.65 (C=O), 1639.49 (C=N), 1589.34 (C=C), 1242.16, 1168.86 and 1056.99 (C-O-C), (C=S) and (C-S-C). Anal. Calcd (%) for $C_{19}H_{13}BrN_4O_2S_2$ (473.36): C, 48.21; H, 2.77; N, 11.84; S, 13.55. Found C, 48.50; H, 2.94; N, 11.99; S, 13.62. HPLC / DAD: Retention time 24.57 min.

(*Z*)-2-thioxo-5-(4-((1-(p-tolyl)-1*H*-1,2,3-triazol-4-yl)methoxy)benzylidene)thiazolidin-4-one **(6f)**

Yield 92%. m.p. 254-256 °C. ^{1}H NMR (400 MHz, DMSO-d_6): δ 13.77 (s, 1H, NH, D_2O exchangeable), 8.92 (s, 1H, triazole-C_5-H), 7.79 (d, *J* = 8.32, 2H, p-tolyl-$C_{2,6}$-H), 7.61 (s, 1H, benzylidene-CH), 7.59 (d, *J* = 8.64 Hz, 2H, benzylidene- $C_{2,6}$-H), 7.40 (d, *J* = 8.32 Hz, 2H, p-tolyl-$C_{3,5}$-H), 7.26 (d, *J* = 8.64 Hz, 2H, benzylidene- $C_{3,5}$-H), 5.34 (s, 2H, OCH_2), 2.38 (s, 3H, CH_3). ^{13}C NMR (100 MHz, DMSO-d_6): δ 196.1, 170.1, 160.4, 143.7, 138.9, 134.8, 133.1, 132.1, 131.8, 130.7, 126.4, 123.4, 120.5, 116.3, 61.8, 21.0. IR (KBr): cm^{-1} 3151.69 (NH), 1701.22 (C=O), 1630 (C=N), 1589.34 (C=C), 1261.45,1172.72 and 1053.13 (C-O-C), (C=S) and (C-S-C). Anal. Calcd (%) for $C_{20}H_{16}N_4O_2S_2$ (408.49): C, 58.81; H, 3.95; N, 13.72; S, 15.70. Found C, 59.09; H, 4.06; N, 13.96; S, 16.02. HPLC / DAD: Retention time 18.11 min.

(*Z*)-5-(4-((1-(4-methoxyphenyl)-1*H*-1,2,3-triazol-4-yl)methoxy)benzylidene)-2-thioxothiazolidin-4-one **(6g)**

Yield 91%. m.p. 256-258 °C. ^{1}H NMR (400 MHz, DMSO-d_6): δ 13.74 (s, 1H, NH, D_2O exchangeable), 8.87 (s, 1H, triazole-C_5-H), 7.81 (d, *J* = 8.64, 2H, benzylidene-$C_{2,6}$-H), 7.62 (s, 1H, benzylidene-CH), 7.59 (d, *J* = 8.4 Hz, 2H, 4-methoxyphenyl-$C_{2,6}$-H), 7.26 (d, *J* = 8.4 Hz, 2H, 4-methoxyphenyl- $C_{3,5}$-H), 7.14 (d, *J* = 8.64 Hz, 2H, benzylidene- $C_{3,5}$-H), 5.33 (s, 2H, OCH_2), 3.84 (s, 3H, OCH_3). ^{13}C NMR (100 MHz, DMSO-d_6): δ 196.1, 170.2, 160.5, 159.8, 143.5, 133.1, 132.0, 130.4, 126.4, 123.5, 123.0, 122.3, 116.3, 115.4, 61.8, 56.0. IR (KBr): cm^{-1} 3140.11 (NH), 1685.79 (C=O), 1620 (C=N), 1589.34 (C=C), 1265.30, 1180.44 and 1041.56 (C-O-C), (C=S) and (C-S-C). Anal. Calcd (%) for $C_{20}H_{16}N_4O_3S_2$ (424.49): C, 56.59; H, 3.80; N, 13.20; S, 15.11. Found C, 56.96; H, 3.97; N, 13.01; S, 15.26. HPLC / DAD: Retention time 11.49 min.

(*Z*)-4-(4-((4-((4-oxo-2-thioxothiazolidin-5-ylidene)methyl)phenoxy)methyl)-1*H*-1,2,3-triazol-1-yl)benzoic acid **(6h)**

Yield 75%. m.p. 278-280 °C. ^{1}H NMR (400 MHz, DMSO-d_6): δ 13.76 (s, 1H, NH, D_2O exchangeable), 13.25 (s, 1H, COOH, D_2O exchangeable), 9.10 (s, 1H, triazole-C_5-H), 8.07-8.16 (m, 4H, 4-carboxyphenyl-Hs), 7.90 (d, *J* = 7.4 Hz, 2H, benzylidene-$C_{2,6}$-H), 7.59-7.62 (m, 1H, benzylidene-CH), 7.29 (d, *J* = 7.4 Hz, 2H, benzylidene-$C_{3,5}$-H), 5.39 (s, 2H, OCH_2). ^{13}C NMR (100 MHz, DMSO-d_6): δ 191.8, 166.8, 163.3, 160.4, 144.2, 139.9, 133.1, 132.3, 131.6, 131.2, 130.5, 123.7, 120.4, 116.3, 115.7, 61.8. IR (KBr): cm^{-1} 3376.71-2792.93 (OH), 3136.25 (NH), 1685.79 (C=O), 1620

(C=N), 1577.77 (C=C), 1257.59, 1165.00 and 1041.56 (C-O-C), (C=S) and (C-S-C). Anal. Calcd (%) for $C_{20}H_{14}N_4O_4S_2$ (438.48): C, 54.79; H, 3.22; N, 12.78; S, 14.62. Found C, 54.85; H, 3.14; N, 13.01; S, 14.50. HPLC / DAD: Retention time 2.74 min.

4.1.2. Click reaction procedure for compounds 5(i,j) and 6(i,j):

To a mixture of 4-propargyloxy-benzylidene thiazolidene-2,4-dione / rhodanine 4 **(a,b)** (1 mmol) and appropriate phenacyl azide (1.5 mmol) in 10 mL of DMF, was added an aqueous solution (5 mL) of sodium ascorbate (0.06 g, 0.34 mmol) and $CuSO_4.5H_2O$ (0.02 g, 0.085 mmol). The mixture was stirred at room temperature for 48h. After cooling, the mixture was poured on ice, filtered, washed with cold water, dried and recrystallized from ethanol/DMF.

(*Z*)-5-(4-((1-(2-(4-chlorophenyl)-2-oxoethyl)-1*H*-1,2,3-triazol-4-yl)methoxy)benzylidene)thiazolidine-2,4-dione **(5i)**

Yield 90%. m.p. 265-266 °C. ^{1}H NMR (400 MHz, DMSO-d_6): δ 12.53 (s, 1H, NH, D_2O exchangeable), 8.24 (s, 1H, triazole-C_5-H), 8.09 (d, J = 8.4 Hz, 2H, 4-chlorophenyl-$C_{2,6}$-H), 7.96 (s, 1H, benzylidene-CH), 7.70 (d, J = 8.4 Hz, 2H, 4-chlorophenyl-$C_{3,5}$-H), 7.59 (d, J = 8.6 Hz, 2H, benzylidene-$C_{2,6}$-H), 7.24 (d, J = 8.6 Hz, 2H, benzylidene-$C_{3,5}$-H), 6.22 (s, 2H, OCH_2), 5.31 (s, 2H, $CO=CH_2$). ^{13}C NMR (100 MHz, DMSO-d_6): δ 191.8, 168.0, 162.8, 160.2, 142.7, 139.6, 133.3, 132.5, 132.1, 130.6, 129.6, 127.0, 126.4, 116.1, 61.8, 56.4. IR (KBr): cm^{-1} 3150 (NH), 1740 (C=O), 1693.50 (amide C=O), 1625 (C=N), 1590 (C=C),1250 and 1040 (C-O-C), (C-S-C). Anal. Calcd (%) for $C_{21}H_{15}ClN_4O_4S$ (454.89): C, 55.45; H, 3.32; N, 12.32; S, 7.05. Found C, 55.81; H, 3.45; N, 12.19; S, 7.18. HPLC / DAD: Retention time 6.51 min.

(*Z*)-5-(4-((1-(2-(4-bromophenyl)-2-oxoethyl)-1*H*-1,2,3-triazol-4-yl)methoxy) benzylidene)thiazolidine-2,4-dione **(5j)**

Yield 87%. m.p. 236-238 °C. ^{1}H NMR (400 MHz, DMSO-d_6): δ 8.24 (s, 1H, triazole-C_5-H), 8.00 (d, J = 7.72 Hz, 2H, 4-bromophenyl-$C_{2,6}$-H), 7.96 (s, 1H, benzylidene-CH), 7.82 (d, J = 7.72 Hz, 2H, 4-bromophenyl-$C_{3,5}$-H), 7.57 (d, J = 8.44 Hz, 2H, benzylidene-$C_{2,6}$-H), 7.24 (d, J = 8.44 Hz, 2H, benzylidene-$C_{3,5}$-H), 6.22 (s, 2H, OCH_2), 5.30 (s, 2H, $CO=CH_2$). ^{13}C NMR (100 MHz, DMSO-d_6): δ 191.9, 168.7, 162.8, 160.2, 142.7, 133.6, 132.5, 132.4, 131.9, 130.6, 128.9, 126.9, 126.4, 121.4, 116.1, 61.8, 56.4. IR (KBr): cm^{-1} 3124.68 (NH), 1735.93 (C=O),1708.93 (amide

C=O), 1658.78 (C=N),1589.34 (C=C), 1240 and 1070 (C-O-C), (C-S-C). Anal. Calcd (%) for $C_{21}H_{15}BrN_4O_4S$ (499.34): C, 50.51; H, 3.03; N, 11.22; S, 6.42. Found C, 50.27; H, 3.16; N, 11.49; S, 6.38. HPLC / DAD: Retention time 7.23 min.

(*Z*)-5-(4-((1-(2-(4-chlorophenyl)-2-oxoethyl)-1*H*-1,2,3-triazol-4-yl)methoxy) benzylidene)-2-thioxothiazolidin-4-one **(6i)**

Yield 89%. m.p. 257-259 °C. ^{1}H NMR (400 MHz, DMSO-d_6): δ 13.62 (s, 1H, NH, D_2O exchangeable), 8.24 (s, 1H, triazole-C_5-H), 8.09 (d, *J* = 8.6 Hz, 2H, 4-chlorophenyl-$C_{2,6}$-H), 7.69 (d, *J* = 8.6 Hz, 2H, 4-chlorophenyl-$C_{3,5}$-H), 7.57-7.59 (m, 3H, benzylidene-CH and benzylidene-$C_{2,6}$-H), 7.25 (d, *J* = 8.84 Hz, 2H, benzylidene-$C_{3,5}$-H), 6.22 (s, 2H, OCH_2), 5.31 (s, 2H, $CO=CH_2$). ^{13}C NMR (100 MHz, DMSO-d_6): δ 196.6, 191.8, 162.8, 160.4, 142.6, 139.6, 133.3, 133.0, 131.6, 130.6, 129.6, 127.0, 126.5, 123.8, 116.2, 61.8, 56.4. IR (KBr): cm^{-1} 3140.11 (NH), 1705.07 (C=O),1651.07 (C=N), 1589.34 (C=C), 1234.44, 1176.58 and 1053.13 (C-O-C), (C=S) and (C-S-C). Anal. Calcd (%) for $C_{21}H_{15}ClN_4O_3S_2$ (470.95): C, 53.56; H, 3.21; N, 11.90; S, 13.62. Found C, 53.80; H, 3.39; N, 12.18; S, 13.90. HPLC / DAD: Retention time 4.22 min.

(*Z*)-5-(4-((1-(2-(4-bromophenyl)-2-oxoethyl)-1*H*-1,2,3-triazol-4-yl)methoxy)benzylidene)-2-thioxothiazolidin-4-one **(6j)**

Ysield 92%. m.p. 236-238 °C. ^{1}H NMR (400 MHz, DMSO-d_6): δ 8.23 (s, 1H, triazole-C_5-H), 8.01 (d, *J* = 8.36 Hz, 2H, 4-bromophenyl-$C_{2,6}$-H), 7.96 (s, 1H, benzylidene-CH), 7.84 (d, *J* = 8.36 Hz, 2H, 4-bromophenyl-$C_{3,5}$-H), 7.56 (d, *J* = 8.72 Hz, 2H, benzylidene-$C_{2,6}$-H), 7.23 (d, *J* = 8.72 Hz, 2H, benzylidene-$C_{3,5}$-H), 6.21 (s, 2H, OCH_2), 5.30 (s, 2H, $CO=CH_2$). ^{13}C NMR (100 MHz, DMSO-d_6): δ 196.6, 167.1, 162.8, 160.1, 142.6, 133.6, 132.7, 132.5, 131.7, 131.1, 130.6, 129.9, 128.9, 126.9, 116.2, 61.8, 56.4. IR (KBr): cm^{-1} 3136.25 (NH), 1697.36 (C=O), 1639.49 (C=N), 1589.34 (C=C), 1240, 1168.86 and 1045.42 (C-O-C), (C=S) and (C-S-C). Anal. Calcd (%) for $C_{21}H_{15}BrN_4O_3S_2$ (515.40): C, 48.94; H, 2.93; N, 10.87; S, 12.44. Found C, 49.21; H, 3.08; N, 11.12; S, 12.71. HPLC / DAD: Retention time 13.47 min.

4.2.Biological Evaluation

4.2.1. *In vitro* COX-1 and COX-2 inhibitory assay:

All the newly synthesized compounds were screened for their ability to inhibit COX-1 and COX-2 enzymes *in vitro*. This was carried out using Cayman colorimetric COX (ovine) inhibitor screening assay kit (Catalog No. 560131) supplied by Cayman

chemicals, Ann Arbor, MI, USA. The preparation of reagents and testing procedures were carried out following the instructions given with the assay kit (Catalog No. 560131) and in agreement with a previously reported method.

4.2.2. *In vitro* 15-LOX inhibitory assay:

The inhibitory activity of the test compounds listed in **Table 1** against soya bean 15-LOX was assessed using Cayman lipoxygenase inhibitor screening assay kit (Catalog No. 760700). The preparation of reagents and testing procedures for determining IC_{50} values of the tested compounds were carried out following the instructions given with the assay kit (Catalog No. 760700) and in agreement with a previously reported method [37].

4.2.3. *In vitro* glucose uptake using rat hemi-diaphragm model*:*

Procedures involving animals and their care were conducted in conformity with the Guide for the Care and Use of Laboratory Animals published by US National Institute of Health (NIH publication No. 83-23, revised 1996) and following the ethical guidelines of Alexandria University on laboratory animals. In all tests, adequate considerations were adopted to reduce pain or discomfort of animals. Reagent preparation and testing procedures for glucose uptake using *in vitro* rat hemi-diaphragm model of the tested compounds were carried out following the instructions in accordance with a previously reported method. In brief, Wistar rats weighing 150-250 g were used (Experimental Animal Centre in Alexandria University). All animals accessed to food and water *ad libitum* and were housed in 12 h dark/light cycle in a controlled condition at 23-25 °C and fasted overnight. The animals were euthanized under ether anesthesia and diaphragms were taken out swiftly avoiding trauma and divided into two halves and weight was noted. The hemi-diaphragms were then rinsed in cold Tyrode solution (without glucose) to remove any blood clots and used accordingly. The glucose content of the working solutions was measured by GOD/POD enzymatic method using VITRO SCIENT glucose kit. The working solutions (n=3) were categorized as follows:

- A negative control that was provided by 2 ml of Tyrode solution with 2000 mg/l

glucose with and without regular insulin (Novo Nordisk, 40 IU/ml) 5 µl containing 0.2 units of insulin.

- Test solutions which contained 2 ml of Tyrode solution with 2000 mg/l glucose and 2 mg of the test compound **4b, 5b, 5e, 5g, 5j, 6b, 6e, 6g, 6j** and **6i** with and without regular insulin (Novo Nordisk, 40 IU/ml) 5 µl containing 0.2 units of insulin.
- A positive control which contained: 2 ml of Tyrode solution with 2000 mg/l glucose and 2 mg of pioglitazone (standard) with and without regular insulin (Novo Nordisk, 40 IU/ml) 5 µl containing 0.2 units of insulin.

4.2.4. Immunohistochemical analysis of ligand-stimulated PPARγ nuclear localization:

Primary rat adipocytes were isolated from perivascular adipose tissue and differentially cultured as described previously [91]. Adipocytes were seeded on sterile coverslips in a 12-well plate at a density of 3000 cells/well. Cells were cultured in DMEM F-12 (Lonza, Basel, Switzerland) containing 10% fetal bovine serum (FBS, Sigma, St. Louis, MO), penicillin (100 U/mL), and streptomycin (100µg/mL); and incubated at 37°C in a humidified atmosphere with 5% CO2 and 95% O_2. Forty-eight hours post seeding, cells were incubated with 10 µM concentration of either pioglitazone, 4b, 5b, 5e, or 5g; or the equivalent amount of the vehicle (DMSO) in triplicates. Following a three-hour exposure interval, treatment media were discarded, cells were washed with phosphate-buffered saline (PBS) and fixed with 2% formaldehyde in PBS for 20 minutes at room temperature. After rinsing with PBS, cells were permeabilized by 0.1% Triton X-100 for 30 minutes at room temperature. Cells were then blocked with 3% normal goat serum (Abcam, Cambridge, UK) in PBS for one hour at room temperature followed by incubation in 1:200 rabbit polyclonal anti-PPARγ (Abcam, Cambridge, UK) in PBS containing 1% normal goat serum overnight at 4°C. Cells were rinsed three times with PBS followed by incubation with 1:100 FITC-conjugated goat anti-rabbit Ig (Abcam, Cambridge, UK) in PBS containing 1% normal goat serum in a light-proof container for one hour at

room temperature. Afterwards, cells were rinsed with PBS and mounted on microscopic slides with Fluoroshield anti-fade mounting medium containing DAPI (Abcam, Cambridge, UK). Negative control slides were prepared by omission of either the primary or the secondary antibodies. Slides were left at 4°C overnight. FITC green fluorescence representing PPARγ staining and DAPI nuclear staining were recorded on an Axiovert Observer Z1 High Resolution Fluorescent Imaging Microscope (Zeiss, Oberkochen, Germany). Fluorescence distribution profiles along line scans in both the FITC and DAPI channels was generated using ImageJ software (National Institutes of Health, Bethesda, MD) to show cellular localization of PPARγ relative to the nucleus.

4.2.5. PPARγ functional reporter gene assay:

HEK293T cells were transiently co-transfected with a hybrid receptor comprising the N-terminal Gal4 DNA binding domain fused to the ligand binding domain of Human PPARγ. The reporter vectors comprise the Renilla luciferase gene functionally linked to the Gal4 upstream activation sequence. Cells were treated with vehicle (DMSO), pioglitazone or test compounds for 24 h. Following the incubation period, treatment media were discarded and luciferase activity was measured using reporter luciferase assay kit according to the manufacturer's instructions and as reported earlier [58]. Luciferase activity was normalized to Renilla luciferase activity and reported as fold induction compared to vehicle. Each experiment was performed in triplicate and repeated at least three times.

4.2.6. Monocyte to macrophage differentiation assay:

THP-1 cells (human acute monocytic leukaemia lineage, American Type Culture Collection, Manassas, VA) were cultured and differentiated as described as described previously [92]. Briefly, cells were cultured in RPMI-1640 (Lonza, Basel, Switzerland) containing 10% FBS, glucose (11 mmol/L), L-glutamine (4 mmol/L), pyruvate (1 mM), penicillin (100 U/mL), and streptomycin (100µg/mL) and incubated at 37°C in a humidified atmosphere of 5% CO2 and 95% air (1). THP-1 monocytes

were seeded at a density of 2 x 10^5 cells/ml in 24-well plates. THP-1 monocytes were differentiated into macrophages by incubation with 25 ng/ml of phorbol myristate-acetate (PMA, Calbiochem, Darmstadt, Germany) for 24 h [93]. Following incubation and cell attachment, supernatants were removed and wells were washed 3x with phosphate-buffered saline. Attached cell density was estimated using a MTS colorimetric cell viability kit (Abcam, Cambridge, UK). Control treatment without PMA was used as a blank. To examine the inhibitory effect of different drugs on the differentiation process, THP-1 cells were incubated with different concentrations of each drug for six hours prior to exposure to PMA. Cell viability readings of attached macrophages in each drug treatment was normalized to the count after PMA exposure following a six-hour incubation with DMSO. Diclofenac was used as a reference COX1/COX2 inhibitor for comparison of the effect of the different compounds on monocyte to macrophage differentiation. All experiments were performed in triplicates. GraphPad Prism software was used to determine IC_{50} values for each compound as the best fit non-linear regression values of the log [inhibitor] vs. response curve. To confirm that the effects observed were a result of interference with the differentiation process rather than monocyte cytotoxicity, THP-1 cell viability at different drug concentrations was assessed prior to the execution of the assay. No change in cell viability was observed for different drug concentrations after 30 h incubation.

4.2.7. IL-1β and TNF-α expression and 20-HETE production assay:

THP-1 cells were seeded at a density of 2.6 x 10^6 cells in T75 culture flasks for western blotting experiments and 3 x 10^5 cells in 6-well plates for the ELISA determination of 2-HETE experiments. Treatment flasks were exposed to 100 μM of the corresponding drug. THP-1 cells were activated with 25 nM PMA for 24 hours followed by a 72-hour challenge with 100 ng/ml LPS. At the end of the challenge period, the conditioned medium was collected from the cell cultures in the 6-well plates, extracted and 20-HETE concentration was measured using an ELISA kit from Detroit R&D Inc. (Detroit, MI, USA) according to the manufacturer instructions. For western blotting, cells in T75 flasks were extracted with a buffer composed of 100 mM dithiothreitol, 1% sodium dodecyl sulphate, 0.9% sodium chloride, and 80 mM

Tris hydrochloride (pH 6.8) as described previously [8]. Sodium dodecyl sulphate polyacrylamide gel electrophoresis, blotting, and antibody labelling was done as described previously [8]. Primary rabbit polyclonal antibodies to IL-1β, TNF-α, and GAPDH were obtained from Abcam (Cambridge, UK). Bands were visualized using Clarity Western ECL substrate (BioRad, Hercules, CA, USA) and a Chemidoc imaging system (BioRad, Hercules, CA, USA). Band density was measured using ImageJ software (National Institutes of Health, Bethesda, MD) and normalized to the GAPDH band density as a loading control.

4.2.8. *In vivo* anti-inflammatory assay:

Adult female albino rats weighing 150-250 g were used (Experimental Animal Center in Alexandria University). All animals were accessed to food and water ad libitum and were housed in 12 h dark/light cycle in a controlled condition at 23-25 ºC. They were allowed to acclimatize for 1 week prior to experimentation. Procedures involving animals and their care were conducted in conformity with the Guide for the Care and Use of Laboratory Animals published by US National Institute of Health (NIH publication No. 83-23, revised 1996) and following the ethical guidelines of Alexandria University on laboratory animals. In all tests, adequate considerations were adopted to reduce pain or discomfort of animals.

Celecoxib and diclofenac sodium (European Egyptian Pharmaceutical industries, Alexandria, Egypt), formalin 5% made from formaldehyde 37% and saline (Merck, Germany) were used. Compounds (**4b, 5b, 5e** and **5g**) were evaluated for their in vivo anti-inflammatory activity applying the formalin-induced rat paw edema screening protocol as an acute inflammation model as reported previously [94].

4.3. Protein purification, crystallization, and structure determination:

The PPARγ LBB was expressed in *E. coli*, purified, and concentrated as described previously [95]. Apo crystals of PPARγ were created by using the hanging drop vapour diffusion method with 500 µL well solution comprising 0.8-1.2M sodium citrate and 0.1M Tris 8.0. The hanging drop was made using 1µL protein plus 1µL well solution. Crystals were cubic, approximately 400microns in each dimension, and

formed within 3 days at 16 ^{o}C. Crystals were soaked with a final concentration of 2mM **4b** in the crystallization well for 2 weeks. Crystals were harvested and transferred to well solution containing 15% ethylene glycol as a cryo-protectant. Crystals were flash cooled by direct submersion into liquid nitrogen and data collection was carried out at beamline MX2 of the Australian Synchrotron. 0.1 degree oscillations were collected using the Eiger 16M detector. Data was processed in XDS [96]. Molecular replacement using Phaser [97], PDB ID: 5U5L [95] as a search model, with ligands and water molecules removed), electron density for **4b** was visible initial difference density maps. Two subunits were found per asymmetric unit. Phenix.refine [98] and Coot [99] were used for refinement and multiple rounds of manual rebuilding. MolProbity was used for structure validation [100]. A Feature Enhanced Map (FEM) $2F_o - F_c$ electron density map was calculated using Phenix to help reduce model bias and improve map quality [101]; an electron density map of the ligand is shown in **Supplementary Information Figure SM2**. Coordinates and structure factors were deposited in the Protein Data Bank under accession code 6E5A. Data processing and refinement statistics can be found in **Supplementary Information Table SM3**.

4.4. Molecular modeling:

4.4.1. Preparation of protein crystal structures:

Coordinates for PPARγ, COX-2, COX-1 and 15-LOX crystal structures was retrieved from the Protein Data Bank (PDB codes: 2PRG, 1CX2, 1EQG and 1LOX, respectively) and handled consequently with Molecular Operating Environment program (MOE 2016.0802) [102]. Redundant chains, non-essential ions, water molecules and ligands were discarded. The default preparation scheme was conducted using “Structure Preparation” module with the default settings. Bond orders, formal charges and explicit hydrogen atoms were added to the complex structure. Subsequently, the most appropriate protonation states and optimization of the H-bond network were performed with the MOE ‘Protonate 3D’ function at standard settings (T = 300 K, pH = 7.0, ionic strength I = 0.1 mol/l). Prepared protein structures were saved as PDB files which were further used for GOLD docking. The PDB files were converted to PDBQT files by employing a python script (*prepare_receptor4.py*)

provided by the MGLTools package (version 1.5.4) for AutoDock Vina (version 1.1.2) and Autodock VinaXB docking experiments. The native geometry of the binding sites was preserved without in-place ligand-protein minimization.

4.4.2. Preparation of the compounds for docking:

The molecules were built and prepared by MOE 2016.0802. 'Molecule wash' function was used to generate meaningful protonation states by deprotonating strong acids and protonating strong bases (if required). Also generating different protomers, conformations and geometrical isomers were allowed at pH 7. Energy minimization of all molecules was performed using the MMFF94x force field at a gradient of 0.01 RMSD (i.e. if the gradient falls below RMSD, the minimization terminates). All possible chiralities were generated (if required) and partial charges were calculated according to the standard parameters of the force field. The resulting structures were saved as SD file for GOLD docking experiments. The SD files were converted and split into PDB files by open-Babel (version 2.3.1) [103], which were further converted into PDBQT files by a MGLTools (version 1.5.4) python script (*prepare_ligand4.py*) for AutoDock Vina and AutoDock VinaXB docking experiments.

4.4.3. Docking experiments:

For GOLD (version 5.2) [43,44] docking, ChemPLP scoring function was used for docking experiments against all the above mentioned targets. Residues of the binding site were defined by specifying the coordinates of the co-crystallized ligands and using a cutoff radius of 10 Å, with the 'detect cavity' option enabled. The scoring function used for GOLD docking experiments was ChemPLP. The search efficiency of the genetic algorithm was at 200%. All the docking solutions were allowed and saved consequently. This docking approach was validated by successful pose-retrieval of the co-crystallized ligand when docked into its corresponding binding site of the crystal structure. All graphical representations for docking poses in the binding sites were rendered using Pymol (v1.1eval) [104] and MOE 2016.0802.

For AutoDock Vina (version 1.1.2) docking against PPARγ, we again employed default docking parameters. The size of the docking grid was generally 20 Å × 20 Å × 20 Å, with a grid spacing of 1 Å. In cases where the ligand binding site was not completely included in the grid box, the grid dimensions were expanded accordingly.

By default, the docking was terminated when the maximum energy difference between the best scored pose and the worst one was 3 kcal/ mol. These settings were also employed for AutoDock VinaXB docking experiments.

4.4.4. pROC-Chemotype plots:

pROC-Chemotype plot [105] is an automated protocol that matches and visualizes ligand chemotype information in combination with the pROC profile obtained by docking, without biasing or modifying the original pROC graph. Cluster number and rank are annotated. For each bioactive molecule, information about the type of data (TOD), the level of activity (LOA), and its bioactivity rank is provided, which also serves as a molecular identifier. The clustering method employed in this protocol is based on Maximum Common Substructures (MCS) of Small Molecule Subgraph Detector (SMSD). In this study we applied the pROC-Chemotype protocol of KNIME [106].

4.5. *In silico* prediction of physicochemical properties, drug-likeness, pharmacokinetic profile and ligand efficiency metrics:

Compounds **4b**, **5b** and **5e** underwent molecular properties prediction by Molinspiration online property calculation toolkit, drug-likeness and solubility parameter calculation by MolSoft software, ADME profiling by PreADMET calculator and Ligand efficiency metrics calculation by Data warrior software.

Notes:

The authors declare no competing financial interest. The PDB code for PPARγ in complex with **4b** is 6E5A. The authors will release the atomic coordinates and the experimental data upon article publication.

References:

[1] S.E. Headland, L. V. Norling, The resolution of inflammation: Principles and challenges, Semin. Immunol. 27 (2015) 149–160. doi:10.1016/j.smim.2015.03.014.

[2] C.N. Serhan, Treating inflammation and infection in the 21st century: New hints from decoding resolution mediators and mechanisms, FASEB J. 31 (2017) 1273–1288. doi:10.1096/fj.201601222R.

[3] V.R. Jala, S.R. Bodduluri, S.R. Satpathy, Z. Chheda, R.K. Sharma, B. Haribabu, The yin and yang of leukotriene B 4 mediated inflammation in cancer, Semin. Immunol. 33 (2017) 58–64. doi:10.1016/j.smim.2017.09.005.

[4] C.S.N. Klose, D. Artis, Innate lymphoid cells as regulators of immunity, inflammation and tissue homeostasis., Nat. Immunol. 17 (2016) 765–74.

doi:10.1038/ni.3489.
[5] C.A. Dinarello, Anti-inflammatory Agents: Present and Future, Cell. 140 (2010) 935–950. doi:10.1016/j.cell.2010.02.043.
[6] S.M. Haffner, The Metabolic Syndrome: Inflammation, Diabetes Mellitus, and Cardiovascular Disease, Am. J. Cardiol. 97 (2006) 3–11. doi:10.1016/j.amjcard.2005.11.010.
[7] N. Esser, S. Legrand-Poels, J. Piette, A.J. Scheen, N. Paquot, Inflammation as a link between obesity, metabolic syndrome and type 2 diabetes, Diabetes Res. Clin. Pract. 105 (2014) 141–150. doi:10.1016/j.diabres.2014.04.006.
[8] O. Al-Assi, R. Ghali, A. Mroueh, A. Kaplan, N. Mougharbil, A.H. Eid, F.A. Zouein, A.F. El-Yazbi, Cardiac Autonomic Neuropathy as a Result of Mild Hypercaloric Challenge in Absence of Signs of Diabetes: Modulation by Antidiabetic Drugs., Oxid. Med. Cell. Longev. 2018 (2018) 9389784. doi:10.1155/2018/9389784.
[9] E. Schauberger, M. Peinhaupt, T. Cazares, A.W. Lindsley, Lipid Mediators of Allergic Disease: Pathways, Treatments, and Emerging Therapeutic Targets, Curr. Allergy Asthma Rep. 16 (2016) 48. doi:10.1007/s11882-016-0628-3.
[10] F.H.G. Tessaro, T.S. Ayala, J.O. Martins, Lipid Mediators Are Critical in Resolving Inflammation: A Review of the Emerging Roles of Eicosanoids in Diabetes Mellitus, Biomed Res. Int. 2015 (2015) 1–8. doi:10.1155/2015/568408.
[11] R. Mashima, T. Okuyama, Redox Biology The role of lipoxygenases in pathophysiology ; new insights and future perspectives, Redox Biol. 6 (2015) 297–310. doi:10.1016/j.redox.2015.08.006.
[12] J.A. Ackermann, K. Hofheinz, M.M. Zaiss, G. Krönke, The double-edged role of 12/15-lipoxygenase during inflammation and immunity, Biochim. Biophys. Acta - Mol. Cell Biol. Lipids. 1862 (2017) 371–381. doi:10.1016/j.bbalip.2016.07.014.
[13] N. Sharma-walia, J. Chandrasekharan, Lipoxins: nature's way to resolve inflammation, J. Inflamm. Res. (2015) 181. doi:10.2147/JIR.S90380.
[14] H. Sadeghian, A. Jabbari, 15-Lipoxygenase inhibitors: a patent review, Expert Opin. Ther. Pat. 26 (2016) 65–88. doi:10.1517/13543776.2016.1113259.
[15] C.D. Funk, Prostaglandins and Leukotrienes: Advances in Eicosanoid Biology, Science (80-.). 294 (2001) 1871–1875. doi:10.1126/science.294.5548.1871.
[16] C. Patrono, B. Rocca, Nonsteroidal antiinflammatory drugs: Past, present and future, Pharmacol. Res. 59 (2009) 285–289. doi:10.1016/j.phrs.2009.01.011.
[17] S. Fiorucci, R. Meli, M. Bucci, G. Cirino, Dual inhibitors of cyclooxygenase and 5-lipoxygenase. A new avenue in anti-inflammatory therapy? 1 1Abbreviations: NSAIDs, nonsteroidal anti-inflammatory drugs; COX, cyclooxygenase; LT, leukotriene; 5-LOX, 5-lipoxygenase; PG, prostaglandin; DFU, 5,5-dimet, Biochem. Pharmacol. 62 (2001) 1433–1438. doi:10.1016/S0006-2952(01)00747-X.
[18] C. Charlier, C. Michaux, Dual inhibition of cyclooxygenase-2 (COX-2) and 5-lipoxygenase (5-LOX) as a new strategy to provide safer non-steroidal anti-inflammatory drugs, Eur. J. Med. Chem. 38 (2003) 645–659. doi:10.1016/S0223-5234(03)00115-6.

[19] T. Hanke, D. Merk, D. Steinhilber, G. Geisslinger, M. Schubert-Zsilavecz, Small molecules with anti-inflammatory properties in clinical development, Pharmacol. Ther. 157 (2016) 163–187. doi:10.1016/j.pharmthera.2015.11.011.
[20] Q. Li, Y.-P. Cheon, A. Kannan, S. Shanker, I.C. Bagchi, M.K. Bagchi, A novel pathway involving progesterone receptor, 12/15-lipoxygenase-derived eicosanoids, and peroxisome proliferator-activated receptor gamma regulates implantation in mice., J. Biol. Chem. 279 (2004) 11570–81. doi:10.1074/jbc.M311773200.
[21] J. Han, L. Sun, Y. Xu, H. Liang, Y. Cheng, Activation of PPARγ by 12/15-lipoxygenase during cerebral ischemia-reperfusion injury, Int. J. Mol. Med. 35 (2015) 195–201. doi:10.3892/ijmm.2014.1998.
[22] A.J. Kroker, J.B. Bruning, Review of the Structural and Dynamic Mechanisms of PPAR γ Partial Agonism, PPAR Res. 2015 (2015) 1–15. doi:10.1155/2015/816856.
[23] M.B. Wright, M. Bortolini, M. Tadayyon, M. Bopst, Minireview: Challenges and Opportunities in Development of PPAR Agonists, Mol. Endocrinol. 28 (2014) 1756–1768. doi:10.1210/me.2013-1427.
[24] S. Yasmin, V. Jayaprakash, Thiazolidinediones and PPAR orchestra as antidiabetic agents: From past to present, Eur. J. Med. Chem. 126 (2017) 879–893. doi:10.1016/j.ejmech.2016.12.020.
[25] V. Capra, M. Bäck, S.S. Barbieri, M. Camera, E. Tremoli, G.E. Rovati, Eicosanoids and Their Drugs in Cardiovascular Diseases: Focus on Atherosclerosis and Stroke, Med. Res. Rev. 33 (2013) 364–438. doi:10.1002/med.21251.
[26] M.T. Mansouri, B. Naghizadeh, B. Ghorbanzadeh, H. Rajabi, M. Pashmforoush, Pharmacological evidence for systemic and peripheral antinociceptive activities of pioglitazone in the rat formalin test: Role of PPARγ and nitric oxide, Eur. J. Pharmacol. 805 (2017) 84–92. doi:10.1016/j.ejphar.2017.03.007.
[27] A. Bornot, U. Bauer, A. Brown, M. Firth, C. Hellawell, O. Engkvist, Systematic exploration of dual-acting modulators from a combined medicinal chemistry and biology perspective, J. Med. Chem. 56 (2013) 1197–1210. doi:10.1021/jm301653f.
[28] N. Chadha, M.S. Bahia, M. Kaur, O. Silakari, Thiazolidine-2,4-dione derivatives: Programmed chemical weapons for key protein targets of various pathological conditions, Bioorganic Med. Chem. 23 (2015) 2953–2974. doi:10.1016/j.bmc.2015.03.071.
[29] M.J. Naim, M.J. Alam, S. Ahmad, F. Nawaz, N. Shrivastava, M. Sahu, O. Alam, Therapeutic journey of 2,4-thiazolidinediones as a versatile scaffold: An insight into structure activity relationship, Eur. J. Med. Chem. 129 (2017) 218–250. doi:10.1016/j.ejmech.2017.02.031.
[30] D. Kaminskyy, A. Kryshchyshyn, R. Lesyk, 5-Ene-4-thiazolidinones – An efficient tool in medicinal chemistry, Eur. J. Med. Chem. 140 (2017) 542–594. doi:10.1016/j.ejmech.2017.09.031.
[31] B.R.P. Kumar, M. Soni, S.S. Kumar, K. Singh, M. Patil, R.B.N. Baig, L. Adhikary, Synthesis, glucose uptake activity and structure-activity relationships

of some novel glitazones incorporated with glycine, aromatic and alicyclic amine moieties via two carbon acyl linker, Eur. J. Med. Chem. 46 (2011) 835–844. doi:10.1016/j.ejmech.2010.12.019.

[32] A.G. Chittiboyina, C.S. Mizuno, P. V. Desai, A. Patny, T.W. Kurtz, H.A. Pershadsingh, R.C. Speth, V. Karamyan, M.A. Avery, Design, synthesis, and docking studies of novel telmisartan–glitazone hybrid analogs for the treatment of metabolic syndrome, Med. Chem. Res. 18 (2009) 589–610. doi:10.1007/s00044-008-9152-x.

[33] T. Yoshioka, T. Fujita, T. Kanai, Y. Aizawa, T. Kurumada, K. Hasegawa, H. Horikoshi, Studies on hindered phenols and analogs. 1. Hypolipidemic and hypoglycemic agents with ability to inhibit lipid peroxidation, J. Med. Chem. 32 (1989) 421–428. doi:10.1021/jm00122a022.

[34] M. Rudnicki, G.L. Tripodi, R. Ferrer, L. Boscá, M.G.R. Pitta, I.R. Pitta, D.S.P. Abdalla, New thiazolidinediones affect endothelial cell activation and angiogenesis, Eur. J. Pharmacol. 782 (2016) 98–106. doi:10.1016/j.ejphar.2016.04.038.

[35] J.R. Santin, F.D.T. Uchôa, M.D.C.A. Lima, M.M. Rabello, I.D. Machado, M.Z. Hernandes, A.A. Amato, F.A. Milton, P. Webb, F.D.A.R. Neves, S.L. Galdino, I.R. Pitta, S.H.P. Farsky, Chemical synthesis, docking studies and biological effects of a pan peroxisome proliferator-activated receptor agonist and cyclooxygenase inhibitor, Eur. J. Pharm. Sci. 48 (2013) 689–697. doi:10.1016/j.ejps.2012.12.029.

[36] J.H. Choi, J.G. Park, H.J. Jeon, M.S. Kim, M.R. Lee, M.N. Lee, S. Sonn, J.H. Kim, M.H. Lee, M.S. Choi, Y.B. Park, O.S. Kwon, T.S. Jeong, W.S. Lee, H.B. Shim, D.H. Shin, G.T. Oh, 5-(4-Hydroxy-2,3,5-trimethylbenzylidene) thiazolidine-2,4-dione attenuates atherosclerosis possibly by reducing monocyte recruitment to the lesion, Exp. Mol. Med. 43 (2011) 471–478. doi:10.3858/emm.2011.43.8.053.

[37] G. Moussa, R. Alaaeddine, L.M. Alaeddine, R. Nassra, A.S.F. Belal, A. Ismail, A.F. El-Yazbi, Y.S. Abdel-Ghany, A. Hazzaa, Novel click modifiable thioquinazolinones as anti-inflammatory agents: Design, synthesis, biological evaluation and docking study, Eur. J. Med. Chem. 144 (2018) 635–650. doi:10.1016/j.ejmech.2017.12.065.

[38] C. Pirat, A. Farce, N. Lebègue, N. Renault, C. Furman, R. Millet, S. Yous, S. Speca, P. Berthelot, P. Desreumaux, P. Chavatte, Targeting Peroxisome Proliferator-Activated Receptors (PPARs): Development of Modulators, J. Med. Chem. 55 (2012) 4027–4061. doi:10.1021/jm101360s.

[39] S. Yasmin, F. Capone, A. Laghezza, F.D. Piaz, F. Loiodice, V. Vijayan, V. Devadasan, S.K. Mondal, Ö. Atll, M. Baysal, A.K. Pattnaik, V. Jayaprakash, A. Lavecchia, Novel Benzylidene Thiazolidinedione Derivatives as Partial PPARγ Agonists and their Antidiabetic Effects on Type 2 Diabetes, Sci. Rep. 7 (2017) 1–17. doi:10.1038/s41598-017-14776-0.

[40] J.C. Silva, F.A. César, E.M. de Oliveira, W.M. Turato, G.L. Tripodi, G. Castilho, A. Machado-Lima, B. de las Heras, L. Boscá, M.M. Rabello, M.Z. Hernandes, M.G.R. Pitta, I.R. Pitta, M. Passarelli, M. Rudnicki, D.S.P. Abdalla, New PPARγ partial agonist improves obesity-induced metabolic

alterations and atherosclerosis in LDLr−/− mice, Pharmacol. Res. 104 (2016) 49–60. doi:10.1016/j.phrs.2015.12.010.

[41] A. Massarotti, S. Aprile, V. Mercalli, E. Del Grosso, G. Grosa, G. Sorba, G.C. Tron, Are 1,4- and 1,5-Disubstituted 1,2,3-Triazoles Good Pharmacophoric Groups?, ChemMedChem. 9 (2014) 2497–2508. doi:10.1002/cmdc.201402233.

[42] M.R. Bauer, T.M. Ibrahim, S.M. Vogel, F.M. Boeckler, Evaluation and Optimization of Virtual Screening Workflows with DEKOIS 2.0 – A Public Library of Challenging Docking Benchmark Sets, J. Chem. Inf. Model. 53 (2013) 1447–1462. doi:10.1021/ci400115b.

[43] G. Jones, P. Willett, R.C. Glen, A.R. Leach, R. Taylor, Development and validation of a genetic algorithm for flexible docking11Edited by F. E. Cohen, J. Mol. Biol. 267 (1997) 727–748. doi:https://doi.org/10.1006/jmbi.1996.0897.

[44] O. Korb, T. Stützle, T.E. Exner, Empirical Scoring Functions for Advanced Protein−Ligand Docking with PLANTS, J. Chem. Inf. Model. 49 (2009) 84–96. doi:10.1021/ci800298z.

[45] O. Trott, A.J. Olson, AutoDock Vina: Improving the speed and accuracy of docking with a new scoring function, efficient optimization, and multithreading, J. Comput. Chem. 31 (2009) 455–461. doi:10.1002/jcc.21334.

[46] M.R. Koebel, G. Schmadeke, R.G. Posner, S. Sirimulla, AutoDock VinaXB: implementation of XBSF, new empirical halogen bond scoring function, into AutoDock Vina, J. Cheminform. 8 (2016) 27. doi:10.1186/s13321-016-0139-1.

[47] C. Patrono, Cardiovascular Effects of Nonsteroidal Anti-inflammatory Drugs, Curr. Cardiol. Rep. 18 (2016) 25. doi:10.1007/s11886-016-0702-4.

[48] Q.H. Chen, P.N. Praveen Rao, E.E. Knaus, Synthesis and biological evaluation of a novel class of rofecoxib analogues as dual inhibitors of cyclooxygenases (COXs) and lipoxygenases (LOXs), Bioorganic Med. Chem. 14 (2006) 7898–7909. doi:10.1016/j.bmc.2006.07.047.

[49] R.O. Meyers, J.D. Lambert, N. Hajicek, A. Pourpak, J.A. Kalaitzis, R.T. Dorr, Synthesis, characterization, and anti-melanoma activity of tetra-O-substituted analogs of nordihydroguaiaretic acid, Bioorg. Med. Chem. Lett. 19 (2009) 4752–4755. doi:10.1016/j.bmcl.2009.06.063.

[50] I. Schneider, F. Bucar, Lipoxygenase inhibitors from natural plant sources. Part 1: Medicinal plants with inhibitory activity on arachidonate 5 lipoxygenase and 5 lipoxygenase [sol] cyclooxygenase, Phyther. Res. 19 (2005) 81–102.

[51] C.D. Sadik, H. Sies, T. Schewe, Inhibition of 15-lipoxygenases by flavonoids: Structure-activity relations and mode of action, Biochem. Pharmacol. 65 (2003) 773–781. doi:10.1016/S0006-2952(02)01621-0.

[52] E. Walaas, O. Walaas, EFFECT OF INSULIN ON RAT DIAPHRAGM UNDER ANAEROBIC CONDITIONS, J. Biol. Chem. . 195 (1952) 367–373.

[53] K. Kar, U. Krithika, Mithuna, P. Basu, S. Santhosh Kumar, A. Reji, B.R. Prashantha Kumar, Design, synthesis and glucose uptake activity of some novel glitazones., Bioorg. Chem. 56 (2014) 27–33. doi:10.1016/j.bioorg.2014.05.006.

[54] T. Umemoto, Y. Fujiki, Ligand-dependent nucleo-cytoplasmic shuttling of peroxisome proliferator-activated receptors, PPARα and PPARγ, Genes to Cells. 17 (2012) 576–596. doi:10.1111/j.1365-2443.2012.01607.x.

[55] V. Maresca, E. Flori, E. Camera, B. Bellei, N. Aspite, M. Ludovici, C. Catricalà, G. Cardinali, M. Picardo, Linking αMSH with PPARγ in B16-F10 melanoma, Pigment Cell Melanoma Res. 26 (2013) 113–127. doi:10.1111/j.1755-148X.2012.01042.x.

[56] B. Bosier, E. Hermans, Promises of Biased Signaling in the Development of Improved Therapeutics, in: Biased Signal. Physiol. Pharmacol. Ther., Elsevier, 2014: pp. 251–292. doi:10.1016/B978-0-12-411460-9.00008-2.

[57] R.M. Cooke, A.J.H. Brown, F.H. Marshall, J.S. Mason, Structures of G protein-coupled receptors reveal new opportunities for drug discovery, Drug Discov. Today. 20 (2015) 1355–1364. doi:10.1016/j.drudis.2015.08.003.

[58] H. Kojo, M. Fukagawa, K. Tajima, A. Suzuki, T. Fujimura, I. Aramori, K. Hayashi, S. Nishimura, Evaluation of Human Peroxisome Proliferator-Activated Receptor (PPAR) Subtype Selectivity of a Variety of Anti-inflammatory Drugs Based on a Novel Assay for PPARδ(β), J. Pharmacol. Sci. 93 (2003) 347–355. doi:10.1254/jphs.93.347.

[59] C. Auffray, D. Fogg, M. Garfa, G. Elain, O. Join-Lambert, S. Kayal, S. Sarnacki, A. Cumano, G. Lauvau, F. Geissmann, Monitoring of blood vessels and tissues by a population of monocytes with patrolling behavior., Science. 317 (2007) 666–70. doi:10.1126/science.1142883.

[60] K.J. Moore, I. Tabas, Macrophages in the pathogenesis of atherosclerosis, Cell. 145 (2011) 341–355. doi:10.1016/j.cell.2011.04.005.

[61] N. Satoh, A. Shimatsu, A. Himeno, Y. Sasaki, H. Yamakage, K. Yamada, T. Suganami, Y. Ogawa, Unbalanced M1/M2 phenotype of peripheral blood monocytes in obese diabetic patients: Effect of pioglitazone, Diabetes Care. 33 (2010) 2010. doi:10.2337/dc09-1315.

[62] M.A. Bouhlel, B. Derudas, E. Rigamonti, R. Dièvart, J. Brozek, S. Haulon, C. Zawadzki, B. Jude, G. Torpier, N. Marx, B. Staels, G. Chinetti-Gbaguidi, PPARγ Activation Primes Human Monocytes into Alternative M2 Macrophages with Anti-inflammatory Properties, Cell Metab. 6 (2007) 137–143. doi:10.1016/j.cmet.2007.06.010.

[63] S. Wallner, M. Grandl, T. Konovalova, A. Sigrüner, T. Kopf, M. Peer, E. Orsó, G. Liebisch, G. Schmitz, Monocyte to macrophage differentiation goes along with modulation of the plasmalogen pattern through transcriptional regulation, PLoS One. 9 (2014). doi:10.1371/journal.pone.0094102.

[64] F.O. Martinez, S. Gordon, M. Locati, A. Mantovani, Transcriptional Profiling of the Human Monocyte-to-Macrophage Differentiation and Polarization: New Molecules and Patterns of Gene Expression, J. Immunol. 177 (2006) 7303–7311. doi:10.4049/jimmunol.177.10.7303.

[65] K. Németh, A. Leelahavanichkul, P.S.T. Yuen, B. Mayer, A. Parmelee, K. Doi, P.G. Robey, K. Leelahavanichkul, B.H. Koller, J.M. Brown, X. Hu, I. Jelinek, R.A. Star, É. Mezey, Bone marrow stromal cells attenuate sepsis via prostaglandin E2–dependent reprogramming of host macrophages to increase their interleukin-10 production, Nat. Med. 15 (2009) 42–49. doi:10.1038/nm.1905.

[66] D.M. Nikolic, M.C. Gong, J. Turk, S.R. Post, Class A scavenger receptor-mediated macrophage adhesion requires coupling of calcium-independent

phospholipase A(2) and 12/15-lipoxygenase to Rac and Cdc42 activation., J. Biol. Chem. 282 (2007) 33405–11. doi:10.1074/jbc.M704133200.

[67] H. Sakamoto, M. Aikawa, C.C. Hill, D. Weiss, W.R. Taylor, P. Libby, R.T. Lee, Biomechanical strain induces class a scavenger receptor expression in human monocyte/macrophages and THP-1 cells: a potential mechanism of increased atherosclerosis in hypertension., Circulation. 104 (2001) 109–114. doi:10.1161/hc2701.091070.

[68] L. Zhang, Y. Li, M. Chen, X. Su, D. Yi, P. Lu, D. Zhu, 15-LO/15-HETE mediated vascular adventitia fibrosis via p38 MAPK-dependent TGF-β., J. Cell. Physiol. 229 (2014) 245–57. doi:10.1002/jcp.24443.

[69] C. Abrial, S. Grassin-Delyle, H. Salvator, M. Brollo, E. Naline, P. Devillier, 15-Lipoxygenases regulate the production of chemokines in human lung macrophages., Br. J. Pharmacol. 172 (2015) 4319–30. doi:10.1111/bph.13210.

[70] C. Liu, D. Xu, L. Liu, F. Schain, A. Brunnström, M. Björkholm, H.-E. Claesson, J. Sjöberg, 15-Lipoxygenase-1 induces expression and release of chemokines in cultured human lung epithelial cells., Am. J. Physiol. Lung Cell. Mol. Physiol. 297 (2009) L196-203. doi:10.1152/ajplung.00036.2008.

[71] Y. Wen, J. Gu, S.K. Chakrabarti, K. Aylor, J. Marshall, Y. Takahashi, T. Yoshimoto, J.L. Nadler, The role of 12/15-lipoxygenase in the expression of interleukin-6 and tumor necrosis factor-alpha in macrophages., Endocrinology. 148 (2007) 1313–22. doi:10.1210/en.2006-0665.

[72] J.N. Walters, J.S. Bickford, D.E. Beachy, K.J. Newsom, J.-D.H. Herlihy, M. V. Peck, X. Qiu, H.S. Nick, cPLA(2)α gene activation by IL-1β is dependent on an upstream kinase pathway, enzymatic activation and downstream 15-lipoxygenase activity: a positive feedback loop., Cell. Signal. 23 (2011) 1944–51. doi:10.1016/j.cellsig.2011.07.002.

[73] E. Gilberg, M. Gütschow, J. Bajorath, X-ray Structures of Target-Ligand Complexes Containing Compounds with Assay Interference Potential, J. Med. Chem. 61 (2018) 1276–1284. doi:10.1021/acs.jmedchem.7b01780.

[74] T. Mendgen, C. Steuer, C.D. Klein, Privileged Scaffolds or Promiscuous Binders: A Comparative Study on Rhodanines and Related Heterocycles in Medicinal Chemistry, J. Med. Chem. 55 (2012) 743–753. doi:10.1021/jm201243p.

[75] T.M. Ibrahim, M.R. Bauer, F.M. Boeckler, Applying DEKOIS 2.0 in structure-based virtual screening to probe the impact of preparation procedures and score normalization, J. Cheminform. 7 (2015) 21. doi:10.1186/s13321-015-0074-6.

[76] G. Carta, A.J.S. Knox, D.G. Lloyd, Unbiasing Scoring Functions: A New Normalization and Rescoring Strategy, J. Chem. Inf. Model. 47 (2007) 1564–1571. doi:10.1021/ci600471m.

[77] Y. Pan, N. Huang, S. Cho, A.D. MacKerell, Consideration of Molecular Weight during Compound Selection in Virtual Target-Based Database Screening, J. Chem. Inf. Comput. Sci. 43 (2003) 267–272. doi:10.1021/ci020055f.

[78] C. Charlier, C. Michaux, Dual inhibition of cyclooxygenase-2 (COX-2) and 5-lipoxygenase (5-LOX) as a new strategy to provide safer non-steroidal anti-inflammatory drugs, 38 (2003) 645–659. doi:10.1016/S0223-5234(03)00115-6.

[79] Molinspiration Cheminformatics, http://www.molinspiration.com/cgi-bin/properties, (n.d.).
[80] M.L.L. C., http://molsoft.com/mprop/, (n.d.).
[81] http://preadmet.bmdrc.org/adme-prediction/, (n.d.).
[82] http://www.openmolecules.org/datawarrior/, (n.d.).
[83] C. Abad-Zapatero, Ligand efficiency indices for effective drug discovery, Expert Opin. Drug Discov. 2 (2007) 469–488. doi:10.1517/17460441.2.4.469.
[84] A.L. Hopkins, C.R. Groom, A. Alex, Ligand efficiency: a useful metric for lead selection, Drug Discov. Today. 9 (2004) 430–431. doi:10.1016/S1359-6446(04)03069-7.
[85] A.L. Hopkins, G.M. Keserü, P.D. Leeson, D.C. Rees, C.H. Reynolds, The role of ligand efficiency metrics in drug discovery, Nat. Rev. Drug Discov. 13 (2014) 105–121. doi:10.1038/nrd4163.
[86] M.E. Kavanagh, M.R. Doddareddy, M. Kassiou, The development of CNS-active LRRK2 inhibitors using property-directed optimisation, Bioorg. Med. Chem. Lett. 23 (2013) 3690–3696. doi:10.1016/j.bmcl.2013.04.086.
[87] I. Wilkening, G. del Signore, C.P.R. Hackenberger, Synthesis of phosphonamidate peptides by Staudinger reactions of silylated phosphinic acids and esters, Chem. Commun. 47 (2011) 349–351. doi:10.1039/C0CC02472D.
[88] E.L. Myers, R.T. Raines, A Phosphine-Mediated Conversion of Azides into Diazo Compounds, Angew. Chemie Int. Ed. 48 (2009) 2359–2363. doi:10.1002/anie.200804689.
[89] H.H. Kinfe, Y.H. Belay, Synthesis and Biological Evaluation of Novel Thiosemicarbazone – Triazole Hybrid Compounds Antimalarial Agents, South African J. Chem. 66 (2013) 130–135.
[90] K. Lal, P. Yadav, A. Kumar, Synthesis, characterization and antimicrobial activity of 4-((1-benzyl/phenyl-1H-1,2,3-triazol-4-yl)methoxy)benzaldehyde analogues, Med. Chem. Res. 25 (2016) 644–652. doi:10.1007/s00044-016-1515-0.
[91] M.E. Fernyhough, J.L. Vierck, G.J. Hausman, P.S. Mir, E.K. Okine, M. V. Dodson, Primary adipocyte culture: Adipocyte purification methods may lead to a new understanding of adipose tissue growth and development, Cytotechnology. 46 (2004) 163–172. doi:10.1007/s10616-005-2602-0.
[92] S.B. Vasamsetti, S. Karnewar, A.K. Kanugula, A.R. Thatipalli, J.M. Kumar, S. Kotamraju, Metformin Inhibits Monocyte-to-Macrophage Differentiation via AMPK-Mediated Inhibition of STAT3 Activation: Potential Role in Atherosclerosis, Diabetes. 64 (2015) 2028–2041. doi:10.2337/db14-1225.
[93] E.K. Park, H.S. Jung, H.I. Yang, M.C. Yoo, C. Kim, K.S. Kim, Optimized THP-1 differentiation is required for the detection of responses to weak stimuli, Inflamm. Res. 56 (2007) 45–50. doi:10.1007/s00011-007-6115-5.
[94] M. Fereidoni, A. Ahmadiani, S. Semnanian, M. Javan, An accurate and simple method for measurement of paw edema, J. Pharmacol. Toxicol. Methods. 43 (2000) 11–14. doi:10.1016/S1056-8719(00)00089-7.
[95] H. Rajapaksha, H. Bhatia, K. Wegener, N. Petrovsky, J.B. Bruning, X-ray crystal structure of rivoglitazone bound to PPARγ and PPAR subtype

selectivity of TZDs, Biochim. Biophys. Acta - Gen. Subj. 1861 (2017) 1981–1991. doi:10.1016/j.bbagen.2017.05.008.
[96] W. Kabsch, Xds, Acta Crystallogr. Sect. D Biol. Crystallogr. 66 (2010) 125–132. doi:10.1107/S0907444909047337.
[97] A.J. McCoy, Solving structures of protein complexes by molecular replacement with Phaser, Acta Crystallogr. Sect. D Biol. Crystallogr. 63 (2006) 32–41. doi:10.1107/S0907444906045975.
[98] P. V. Afonine, R.W. Grosse-Kunstleve, N. Echols, J.J. Headd, N.W. Moriarty, M. Mustyakimov, T.C. Terwilliger, A. Urzhumtsev, P.H. Zwart, P.D. Adams, Towards automated crystallographic structure refinement with phenix.refine, Acta Crystallogr. Sect. D Biol. Crystallogr. 68 (2012) 352–367. doi:10.1107/S0907444912001308.
[99] P. Emsley, B. Lohkamp, W.G. Scott, K. Cowtan, Features and development of Coot, Acta Crystallogr. Sect. D Biol. Crystallogr. 66 (2010) 486–501. doi:10.1107/S0907444910007493.
[100] C.J. Williams, J.J. Headd, N.W. Moriarty, M.G. Prisant, L.L. Videau, L.N. Deis, V. Verma, D.A. Keedy, B.J. Hintze, V.B. Chen, S. Jain, S.M. Lewis, W.B. Arendall, J. Snoeyink, P.D. Adams, S.C. Lovell, J.S. Richardson, D.C. Richardson, MolProbity: More and better reference data for improved all-atom structure validation, Protein Sci. 27 (2018) 293–315. doi:10.1002/pro.3330.
[101] P. V. Afonine, N.W. Moriarty, M. Mustyakimov, O. V. Sobolev, T.C. Terwilliger, D. Turk, A. Urzhumtsev, P.D. Adams, FEM: Feature-enhanced map, Acta Crystallogr. Sect. D Biol. Crystallogr. 71 (2015) 646–666. doi:10.1107/S1399004714028132.
[102] N. Demirbas, S.A. Karaoglu, A. Demirbas, K. Sancak, Synthesis and antimicrobial activities of some new 1-(5-phenylamino-[1,3,4]thiadiazol-2-yl)methyl-5-oxo-[1,2,4]triazole and 1-(4-phenyl-5-thioxo-[1,2,4]triazol-3-yl)methyl-5-oxo- [1,2,4]triazole derivatives, Eur. J. Med. Chem. 39 (2004) 793–804. doi:https://doi.org/10.1016/j.ejmech.2004.06.007.
[103] N.M. O'Boyle, M. Banck, C.A. James, C. Morley, T. Vandermeersch, G.R. Hutchison, Open Babel: An open chemical toolbox, J. Cheminform. 3 (2011) 33. doi:10.1186/1758-2946-3-33.
[104] L. Delano Scientific, The PyMOL Molecular Graphics System, Version 1.1eval, (2008).
[105] T.M. Ibrahim, M.R. Bauer, A. Dörr, E. Veyisoglu, F.M. Boeckler, pROC-Chemotype Plots Enhance the Interpretability of Benchmarking Results in Structure-Based Virtual Screening, J. Chem. Inf. Model. 55 (2015) 2297–2307. doi:10.1021/acs.jcim.5b00475.
[106] M.R. Berthold, N. Cebron, F. Dill, T.R. Gabriel, T. Kötter, T. Meinl, P. Ohl, C. Sieb, K. Thiel, B. Wiswedel, KNIME: The Konstanz Information Miner BT - Data Analysis, Machine Learning and Applications, in: C. Preisach, H. Burkhardt, L. Schmidt-Thieme, R. Decker (Eds.), Springer Berlin Heidelberg, Berlin, Heidelberg, 2008: pp. 319–326.

Research highlights:

- A novel series of 1,2,3-triazolyl-thiazolidinedione/rhodanine hybrids was rationally designed as multi-target glitazone-like PPARγ partial agonists/COX-2 and 15-LOX inhibitors.
- COX-2 and 15-LOX in vitro assays identified 10 compounds as dual inhibitors.
- Glucose uptake assay recognized 6 compounds as insulin-sensitive and 2 compounds as insulin-independent uptake enhancers.
- PPARγ agonistic activity was confirmed via reporter assay and immunohistochemical analysis.
- 4 Compounds showed potent inhibition of monocyte to macrophage differentiation as well as high *in vivo* anti-inflammatory activity.
- Crystal structure of PPARγ ligand binding domain (LBD) in complex with the most active compound has been solved and demonstrated partial agonistic behavior.